Cell Reports

Resource

Quantitative Map of Proteome Dynamics during Neuronal Differentiation

Graphical Abstract

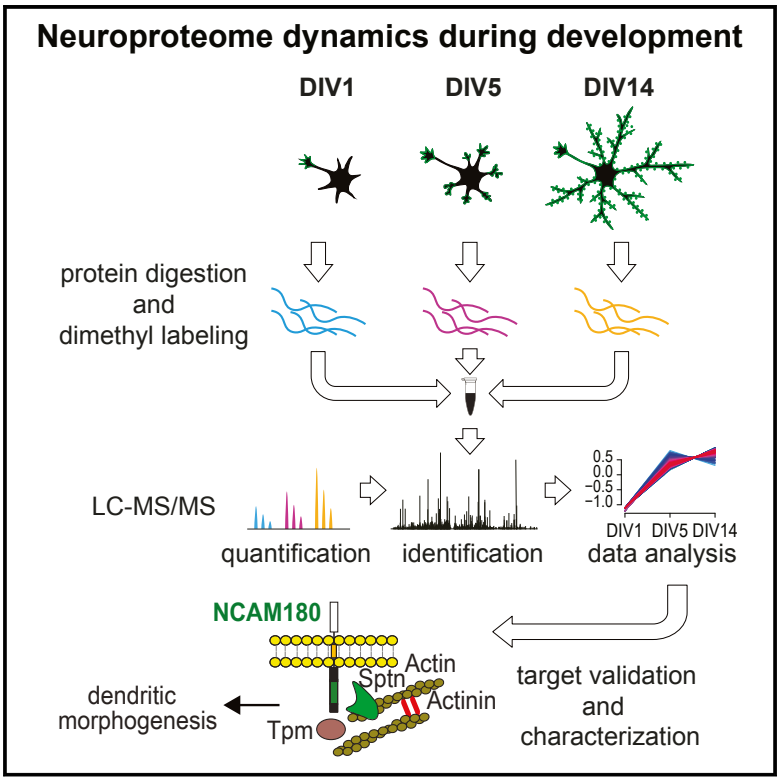

Authors

Christian K. Frese, Marina Mikhaylova, Riccardo Stucchi, ..., Albert J.R. Heck, A.F. Maarten Altelaar, Casper C. Hoogenraad

Correspondence

m.altelaar@uu.nl (A.F.M.A.), c.hoogenraad@uu.nl (C.C.H.)

In Brief

In this study, Frese et al. generate a systematic quantitative map of proteome dynamics during the specific stages of rat hippocampal neuron development in vitro. Six expression profile clusters give a comprehensive overview of protein abundances over time, providing a database of stage-specific protein expression patterns in neurons.

Highlights

- Systematic profile of proteome dynamics throughout neuronal development in vitro
- Approximately 1,800 proteins show significant expression changes during differentiation
- Six expression profile clusters describe stage-specific patterns of protein dynamics
- This protein database may help to identify neurodevelopment mechanisms

Accession Numbers

PXD005031

Frese et al., 2017, Cell Reports *18*, 1527–1542
February 7, 2017
http://dx.doi.org/10.1016/j.celrep.2017.01.025

CellPress

Cell Reports
Resource

Quantitative Map of Proteome Dynamics during Neuronal Differentiation

Christian K. Frese,[1,2,4,5] Marina Mikhaylova,[3,4,6] Riccardo Stucchi,[1,2,3,4] Violette Gautier,[1,2,7] Qingyang Liu,[1,2,3] Shabaz Mohammed,[1,2,8] Albert J.R. Heck,[1,2] A.F. Maarten Altelaar,[1,2,*] and Casper C. Hoogenraad[3,9,*]

[1]Biomolecular Mass Spectrometry and Proteomics, Bijvoet Center for Biomolecular Research and Utrecht Institute for Pharmaceutical Sciences, Utrecht University, Padualaan 8, 3584 Utrecht, the Netherlands
[2]Netherlands Proteomics Centre, Padualaan 8, 3584 Utrecht, the Netherlands
[3]Cell Biology, Department of Biology, Faculty of Science, Utrecht University, 3584 Utrecht, the Netherlands
[4]Co-first author
[5]Present address: CECAD Research Center, University of Cologne, Joseph-Stelzmann-Str. 26, 50931 Cologne, Germany
[6]Present address: Center for Molecular Neurobiology, ZMNH, University Medical Center Hamburg-Eppendorf, 20251 Hamburg, Germany
[7]Present address: Evotec France, 195 Route d'Espagne, BP13669, 31036 Toulouse, France
[8]Present address: Department of Biochemistry, University of Oxford, South Parks Road, OX13QU Oxford, UK
[9]Lead Contact
*Correspondence: m.altelaar@uu.nl (A.F.M.A.), c.hoogenraad@uu.nl (C.C.H.)
http://dx.doi.org/10.1016/j.celrep.2017.01.025

SUMMARY

Neuronal differentiation is a multistep process that shapes and re-shapes neurons by progressing through several typical stages, including axon outgrowth, dendritogenesis, and synapse formation. To systematically profile proteome dynamics throughout neuronal differentiation, we took cultured rat hippocampal neurons at different developmental stages and monitored changes in protein abundance using a combination of stable isotope labeling and high-resolution liquid chromatography-tandem mass spectrometry (LC-MS/MS). Almost one third of all 4,500 proteins quantified underwent a more than 2-fold expression change during neuronal differentiation, indicating extensive remodeling of the neuron proteome. To highlight the strength of our resource, we studied the neural-cell-adhesion molecule 1 (NCAM1) and found that it stimulates dendritic arbor development by promoting actin filament growth at the dendritic growth cone. We anticipate that our quantitative map of neuronal proteome dynamics is a rich resource for further analyses of the many identified proteins in various neurodevelopmental processes.

INTRODUCTION

The ability to generate in vitro cultures of primary rat or mouse neuronal cells has been fundamental to advancing our understanding of the development and functioning of the nervous system. A major advantage of performing experiments in primary hippocampal culture systems is that neurons resynchronize in culture prior to further differentiation (Dotti et al., 1988). This allows systematic processing and analyses of neuronal populations at the same developmental stage, which is particularly helpful for global system-wide analyses. Pyramidal neurons, the principal neuronal cell type in the hippocampus, account for the vast majority of the total neuronal cell population within these preparations and express many key phenotypic features of various neuronal cell types. The stages of neuron development in culture have been categorized and provide a starting point for studying neurodevelopmental processes, such as neuronal polarity, dendrite development, and synapse formation (Dotti et al., 1988). Directly after plating and attaching to the substrate, the cells develop lamellipodia around the soma (stage 1) that, within a few hours, transform into several short and highly motile neurites (stage 2). Quickly after, the neurons polarize upon which one of the several neurites develops into an axon (stage 3). Around day in vitro (DIV) 4 (DIV4), dendrites start to develop from the minor neurites (stage 4); this process is much slower than axonal outgrowth and specification and lasts for several days. After 1 week in culture, synaptogenesis begins, and neurons form functional synaptic contacts and, in the following weeks, undergo further neuronal maturation (stage 5).

Several studies have been reported monitoring global gene expression changes in developing rodent neurons (Mody et al., 2001; Dabrowski et al., 2003), albeit nearly all at the mRNA transcript level. These studies revealed that large changes in mRNA expression occur across different stages of hippocampal neuronal development (Dabrowski et al., 2003). Several earlier studies have been reporting differential gene expression during the specialization of the axon and dendrites in hippocampal primary culture systems. In more recent studies, also, the expression of non-coding regulatory RNAs has been profiled in developing neurons (van Spronsen et al., 2013). Transcriptome analysis of different brain regions and different cell types, including cortical primary neurons, has been compared with data from large-scale quantitative proteomic screens (Sharma et al., 2015). However, in many cases, the gene expression changes measured with transcriptomics approaches do not

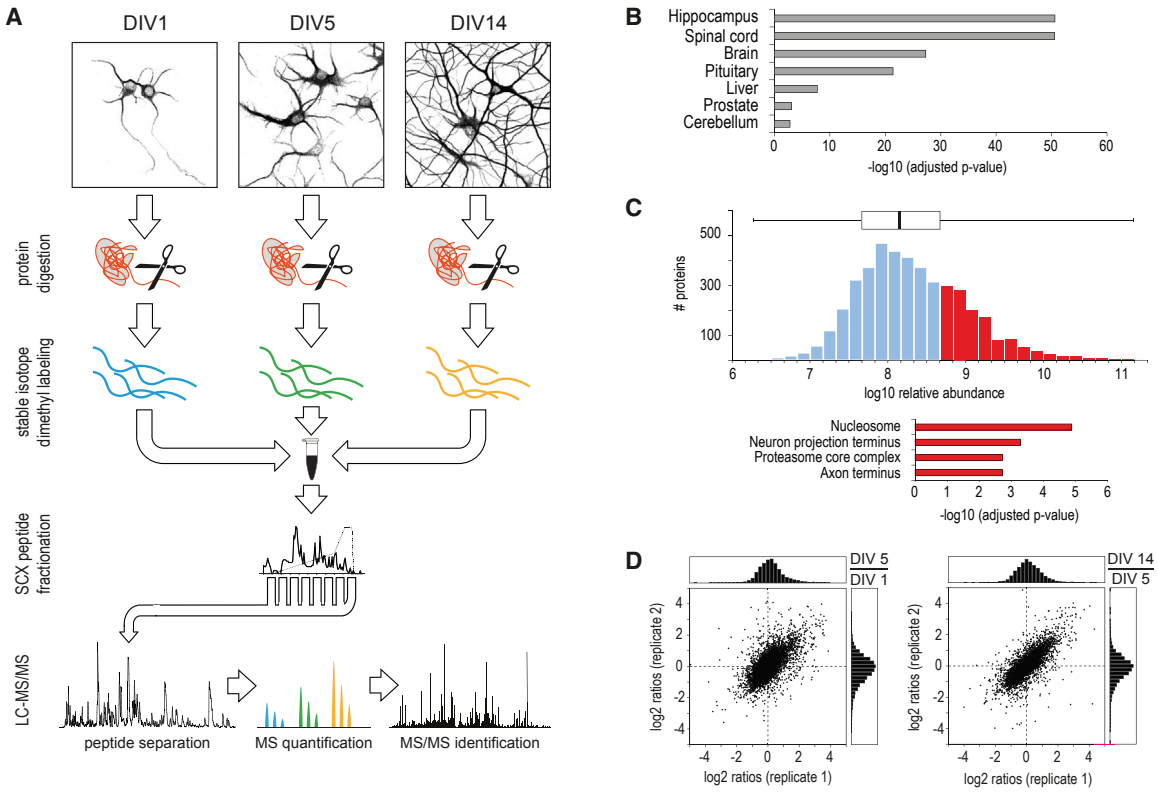

Figure 1. MS-Based Quantitative Proteomic Analysis of Developing Hippocampal Neurons in Culture

(A) Workflow of quantitative neuroproteomic analysis.

(B) Tissue enrichment analysis of all identified proteins using the Database for Annotation, Visualization, and Integrated Discovery (DAVID).

(C) Distribution of protein abundances, spanning five orders of magnitude.

(D) In total, 4,354 proteins were quantified across all time points, and good correlation between biological replicates is observed.

See also Table S1.

completely reflect the changes measured at the protein level. Several studies have shown that the correlation between mRNA and protein expressions can be low due to several factors such as protein turnover, half-lives, and other post-transcription mechanisms (Low et al., 2013). Moreover, a single mRNA can be translated multiple times, introducing another level of complexity in correlating such data. In this context, we argue that applying advanced MS methods and quantitative proteomics approaches to systematically profile protein expression during neuronal differentiation will provide a better proxy for changes in protein expression.

Here, we perform a systematic and in-depth proteome analysis of hippocampal neurons in culture and established a quantitative map of neuron-specific proteome dynamics during developmental stages 2–3, 4, and 5. Our dataset comprises 6,753 protein identifications, of which more than 4,300 were quantified over all time points, covering crucial neuronal developmental processes, including axon outgrowth, dendrite formation, and synaptogenesis. About one third of the proteins reveal substantial changes in protein expression throughout the neuronal differentiation, clearly highlighting the extensive reprogramming of the proteome. Our analysis revealed an unappreciated role for neural-cell-adhesion molecule 1 isoform 180 (NCAM180) in dendritic development. NCAM180 is strongly upregulated during dendrite outgrowth, is highly enriched in dendritic growth cones, and interacts with a large variety of actin-binding proteins.

RESULTS

Global Proteomic Signatures of Developing Hippocampal Neurons

To profile neuronal proteome alterations during differentiation, primary hippocampal neurons were grown in serum-free neurobasal medium, enabling rapid differentiation and maturation (Dotti et al., 1988). Cells were harvested after DIV1, DIV5, and DIV14, corresponding to neuronal developmental stages 2–3, 4, and 5, respectively, as described recently (van Spronsen et al., 2013). These stages are associated with the distinct neuronal differentiation processes axon formation and specification (stages 2–3/DIV1), dendrite outgrowth (stage 4/DIV5), synaptogenesis, and maturation (stage 5/DIV14). For in-depth quantitative proteome analysis, cell lysates of the three time points were subjected to tryptic digestion (Figure 1A), triplex stable-isotope dimethyl labeling (Boersema et al., 2009), strong cation-exchange (SCX)-based fractionation, and nano-ultra-performance liquid

chromatography (nano-UPLC) coupled to high-resolution liquid chromatography-tandem mass spectrometry (LC-MS/MS). Quantification of relative protein expression changes was performed based on the MS signal intensities of the stable-isotope-labeled peptide ions (Figure 1A). In total, 46,869 unique peptides from 6,753 unique proteins were identified (median unique peptides per protein = 6.9). Tissue enrichment analysis against the whole *Rattus norvegicus* proteome as background revealed that the dataset covers large parts of hippocampal neuron-specific proteins (Fisher's exact test, adjusted p = 2.3E−51; Figure 1B). Overall, 4,354 proteins were quantified across all time points (median ratio count = 14; Table S1). The averaged relative protein abundances span five orders of magnitude (Figure 1C). Within the 25% most abundant proteins, we observed numerous neuron-specific proteins. Gene Ontology (GO) enrichment analysis, with respect to cellular component, highlights proteins located in the axon and nerve terminal ("neuron projection terminus") as being among the most abundant proteins, besides more commonly detected nucleosomal proteins and the proteasome (Figure 1C). Scatterplots of the $\log_2$-transformed protein ratios (DIV5/DIV1 and DIV14/DIV5) and a heatmap of Pearson correlation scores illustrate the good correlation between biological replicates (Figure 1D; Figure S1A). In total, 1,793 proteins show more than 2-fold ($\log_2$ scale < -1 and >1) expression changes, indicating extensive remodeling of at least one third of the neuron proteome during differentiation (Figure S1B).

Quantitative Analysis of Proteome Dynamics during Neuron Differentiation

We assessed the global proteome changes of 4,354 proteins quantified across all time points. Close inspection of proteins that were considered not significantly changing (Supplemental Experimental Procedures) revealed general protein metabolism and catabolism as the main processes that are not substantially differentially regulated during neuronal differentiation. This is reflected by several GO terms, such as "translation" (adjusted p value 9.8E-8) and "protein catabolic process" (p = 7.5E−6), and the Kyoto Encyclopedia of Genes and Genomes (KEGG) terms "ribosome" (p = 9.9E−5) and "proteasome" (p = 6.8E−4) that were found overrepresented (Figure S1C). Together, these findings imply that the global protein turnover rates are not substantially affected in the course of proteome remodeling during neuronal differentiation.

To obtain an unbiased view of the proteome expression dynamics during neuronal differentiation, we performed unsupervised fuzzy clustering of all significantly changing proteins. This analysis resulted in six clusters of distinct expression profiles (Figure 2A), with proteins upregulated during differentiation in clusters 1, 2, and 3 and proteins downregulated present in clusters 4, 5, and 6. We next investigated whether the clusters revealed proteins with developmental stage-specific expression patterns. Indeed, many proteins within specific clusters shared functionalities related to their cellular component, molecular function, or their contribution to distinct biological processes (Figure 2B). Complete GO annotations for each cluster can be found in Figure S2.

Cluster 6 contains proteins strongly downregulated from DIV1 to DIV5 and, to a lesser extent, from DIV5 to DIV14, indicating a precisely timed downregulation during early neuronal differentiation. Proteins in this cluster are mainly involved in early differentiation processes of post-mitotic neurons, which do not proliferate and remain arrested in G0 phase, exemplified by multiple proteins involved in the regulation of cell cycle and DNA replication, such as DNA helicases. This includes minichromosome maintenance complex proteins (Mcm2–Mcm7) as well as DNA polymerase delta (Pold2), replication factor 5 (Rfc5), and Flap endonuclease 1 (Fen1) (Figure 2C). Downregulation of proteins related to cell cycle and DNA replication have been similarly observed in other terminally differentiating cells (Kristensen et al., 2013). In line with these findings, we detected slight upregulation of cyclin-dependent kinase 5 (Cdk5) (Figure S3A), which is known to be exclusively expressed in post-mitotic neurons and is involved in suppressing cell-cycle reentry (Zhang and Herrup, 2011).

Proteins in cluster 4 exhibit a strong downregulation from DIV5 to DIV14 (Figure 2A). Many proteins in this cluster are associated with RNA metabolism (Figure 2B), exemplified by a highly connected group of mRNA polyadenylation factors (Figure 2C). Interestingly, several transcription factors, which play key roles in neuronal differentiation, are also allocated to this cluster. A prominent example of this subset of proteins is the neuron-specific transcription factor Sox11, which is the most downregulated protein in the total dataset (expression level decreases about 40-fold from DIV1 to DIV14; see also Figures 4A and 4B). The onset of Sox11 expression is known to overlap with decreased expression of Sox2 (not quantified in our data) in neuronal committed proliferating progenitor cells, promoting differentiation into premature neurons (Haslinger et al., 2009). Likewise, transcription factor Bcl11a, which has been identified as a negative regulator of axon branching and dendrite outgrowth (Kuo et al., 2009), follows the expression profile of cluster 4. Other related transcription factors are allocated to cluster 5 (sustained decrease of relative protein levels from DIV1 to DIV14); for instance, Foxg1 and Sox11-interacting protein Pou3f2, both of which play important roles in the early to mid-neurogenesis of postmitotic neurons (Dominguez et al., 2013; Hsieh, 2012). Another transcription factor found in cluster 5 is Tbr1, which is expressed in early postmitotic neurons, promotes neurogenesis, and functions as a repressor of astrocyte formation (Méndez-Gómez et al., 2011). Moreover, Tbr1 has been reported to be involved in regulation of axon pathfinding (Hevner et al., 2006), a process that is part of the major developmental changes from stage 2 to stage 3. Collectively, our data show that neuronal differentiation and maturation from stages 2–3 to stage 5 resonate with a gradual decrease of several transcription factors that are key regulators in the early events of neurogenesis and initial axon formation. Notably, Sox8, another member of the SRY-related HMG (high-mobility group)-box gene family, shows a minor increase from DIV1 to DIV5 and an elevated increase from DIV5 to DIV14 (cluster 1). Sox8 is reportedly involved in the regulation of terminal differentiation of oligodendrocytes (Stolt et al., 2004). Late upregulation from developmental stage 4 to stage 5 suggests that Sox8 might also be involved in the terminal differentiation of neurons. However, its functional role in the later stages of neuronal development remains to be unveiled.

Cluster 5, representing a constant decrease of relative protein levels over time (Figure 2A), is enriched for proteins associated to

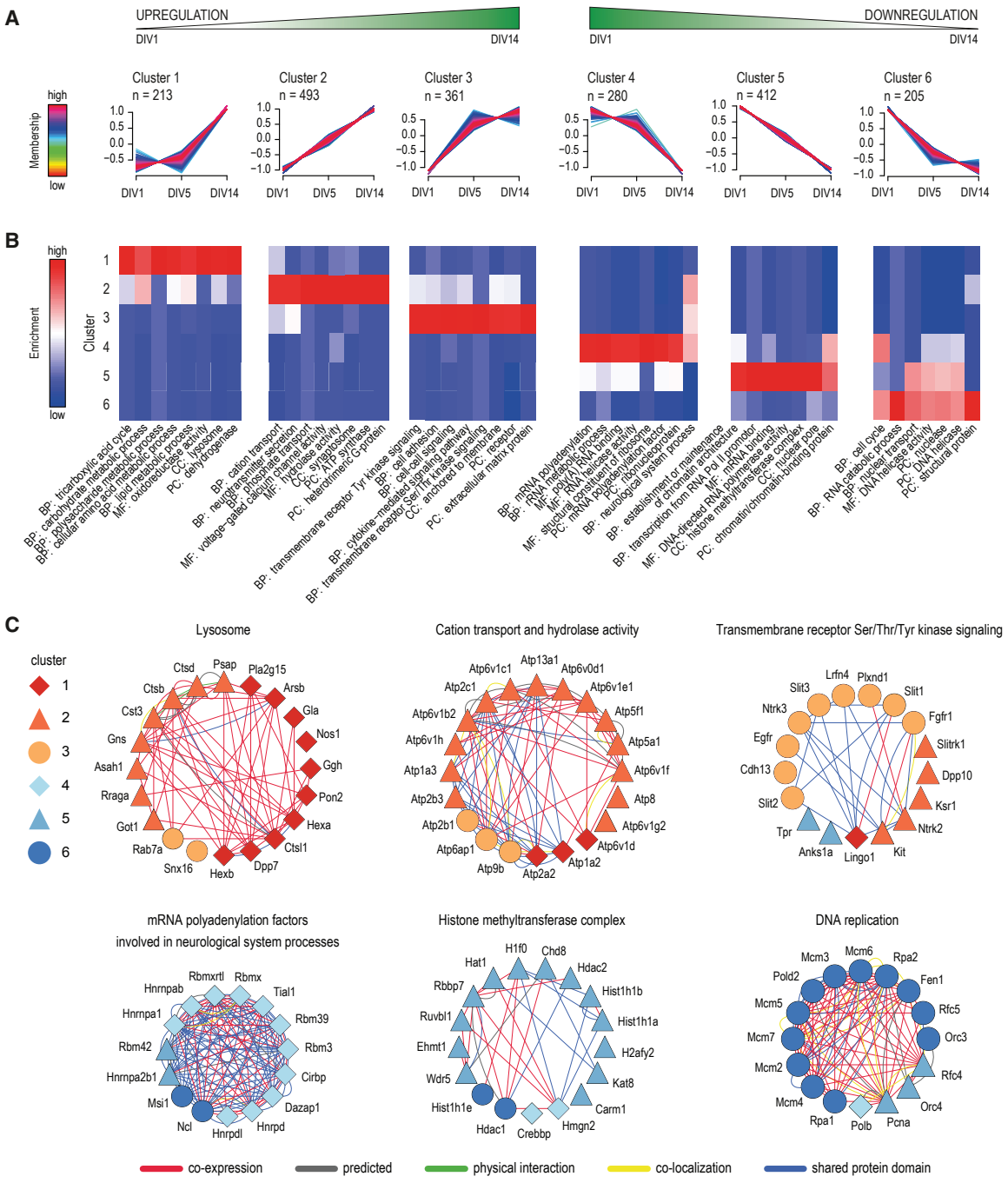

Figure 2. Dynamic Proteome Remodeling during Neuronal Differentiation

(A) Unsupervised clustering of proteome dynamics revealed six clusters with distinct protein expression profiles. n represents the number of proteins per cluster.

(B) Gene ontology enrichment analysis of each cluster was performed using a Fisher's exact test (cutoff $p < 0.002$, Benjamini-Hochberg corrected). Representative biological processes (BP), molecular functions (MF), cellular components (CC), and protein classes (PC) that are overrepresented in one of the clusters are visualized.

(C) Protein network analysis showing highly connected proteins that are representative for each cluster.

chromatin (Figure 2B). Steady downregulation of histone methyltransferases (Ehmt1 and Wdr5), acetyltransferases (Kat8 and Hat1), and histones (Hist1h1b, Hist1h1a, and H2afy2) indicate an ongoing remodeling of the chromatin architecture during neuronal differentiation (Figure 2C). The GO term "mRNA binding" was also found specifically enriched in cluster 5. In fact, 42 out of 103 proteins classified as RNA-binding proteins (RBPs) (Table S2) are allocated to this cluster and undergo, on

average, 3-fold downregulation (log_2 scale = −1.6) from DIV1 to DIV14. Post-transcriptional regulation by RBPs controls gene expression and diversification and is known to accurately coordinate spatiotemporal differentiation of neurons (DeBoer et al., 2013). A prominent member of this cluster is Polypyrimidine tract-binding protein 2 (Ptbp2). Ptbp2 is predominantly expressed in brain tissue during the early stages of neurogenesis, and its main function is the precisely timed negative regulation of alternative splicing events of a distinct set of target genes that play key roles in neuronal differentiation (Sawicka et al., 2008). Therefore, we mined our data for proteins whose transcripts are targets of Ptbp2 (Licatalosi et al., 2012). We observed that the decrease in Ptbp2 levels coincides with increased expression of several proteins whose transcripts are targets of Ptbp2 (including Camk2b, Camk2g, Psd95, Dnm1, Ppp3cb, and Numb). Interestingly, we observed for three other target proteins, whose transcript levels were found elevated in that study, no significant expression changes (Sorbs2 and Pum2) or only a slight decrease (Sympk, cluster 5) in our dataset. Notably, the neuron-specific RBPs Nova1 and Nova2, which are direct interactors of Ptbp2, show no significant expression change from DIV1 to DIV14. Among the upregulated RBPs are Pura and Purb, which, besides their molecular function in RNA binding, are known transcriptionally active DNA binders. Pura and Purb undergo a highly similar expression increase from DIV5 to DIV14 (cluster 1), indicating a specific role in synapse formation and later maturation processes. Indeed, reduced synapse formation was observed in Pura knockout mice (White et al., 2009), supporting a presumed role during synaptogenesis. Notably, a third member of the Pur family, Purg, shows stronger and earlier upregulation compared to Pura and Purb, suggesting involvement in differentiation events preceding synapse formation. Together, these findings support highly coordinated reorganization of the protein network orchestrating post-transcriptional gene expression regulation during neuronal differentiation (Loya et al., 2010).

The proteins in cluster 1 show a substantial increase in relative expression levels from DIV5 to DIV14 (Figure 2A). This expression profile corresponds to stage-specific upregulation during maturation from stage 4 to stage 5. Distinct GO terms, which were found enriched in cluster 1, cover proteins involved in several metabolic processes, including polysaccharide, amino acid, and lipid metabolism (Figure 2B). Closer inspection of the corresponding proteins revealed that most of them function as catalytic enzymes in lysosomes (e.g., cathepsin L1, arylsulfatase B, and dipeptidyl peptidase 2; Figure 2C). Endosomal trafficking is a key control mechanism in synapse formation and modulation of synaptic plasticity. For example, postsynaptic receptor density is governed by the interplay of endosomal recycling and endosome-lysosome trafficking. Therefore, the observed upregulation of lysosomal proteins in the course of neuronal development could reflect an increase in the cellular capacity for the degradation via the lysosomal pathway.

Cluster 3 comprises proteins that undergo increased expression from DIV1 to DIV5, while the expression changes from DIV5 to DIV14 are marginal (Figure 2A). Many proteins in this cluster are associated with cell adhesion and cell-cell signaling-related GO terms (Figure 2B). This includes several transmembrane receptor kinases involved in cell adhesion, migration, axon guidance, and dendrite formation. For instance, prominent members of this cluster are growth factor receptors Egfr and Fgfr1; neurotrophin receptor Ntrk3; semaphorin receptor Plxnd1; and axon guidance cues Slit1, Slit2, and Slit3 (Figure 2C). Moreover, numerous cell-adhesion proteins also follow the expression pattern of cluster 3, which will be discussed in detail later.

Cluster 2 represents a group of proteins whose expression levels constantly increase from DIV1 to DIV5 and from DIV5 to DIV14 (Figure 2A). GO analysis revealed the enrichment of several terms related to cation transport and neurotransmitter secretion in this cluster (Figure 2B), as exemplified by several highly connected subunits of various ATPases (Figure 2C). Furthermore, the majority of the significantly regulated synaptic proteins belong to this cluster (GO term "synaptosome"), which will be discussed in the following sections.

Coordinated Proteome Dynamics of Proteins in Complexes during Differentiation

We next sought to characterize concerted dynamics of proteins within previously annotated protein complexes. Statistical assessment of the significance of co-regulated proteins revealed coordinated expression changes for proteins involved in several cellular processes during neuronal development (Table S3). This includes, for example, nuclear transport (nuclear pore complex), cell-cycle control (anaphase-promoting complex, APC/C), and DNA replication (MCM complex) (all ps < 0.005; Figure 3A), providing further evidence for continuous chromatin remodeling during terminal differentiation of post-mitotic neurons. Conversely, the same statistical analysis can reveal proteins that deviate from the expression profile of the corresponding complex or family, indicating a neuron- or developmental stage-specific function. This is nicely illustrated by expression profile analysis of SNARE proteins from the syntaxin family, revealing neuron-specific expression. Syntaxin proteins are important players in vesicle docking and fusion with target membranes. We observed continuous upregulation of Stx1a and Stx1b from DIV1 to DIV14 (Figure 3B; Figure S3B), both of which are specifically expressed in neuronal and secretory cells, playing a key role in neurotransmitter secretion. All other syntaxins undergo no substantial expression changes (Figure 3B; Figure S3B), indicating that syntaxin-mediated intracellular transport processes, including endosomal (Stx7, Stx8, and Stx12), endoplasmic-reticulum (ER)-to-Golgi- (Stx5 and Stx18), and trans-Golgi (Stx6 and Stx16) trafficking, are not regulated by expression changes of syntaxins in the course of neuronal differentiation.

Next, we determined whether this approach was able to resolve neuron-specific isoforms that modulate distinct functions within protein complexes. Adaptor protein (AP) complexes are involved in intracellular vesicular transport and cargo selection by binding to sorting signals. The AP2 complex mainly plays a role in endocytosis from the plasma membrane, whereas AP3 is important for trans-Golgi sorting events (Boehm and Bonifacino, 2001). All subunits of the AP2 adaptor complex show a significant ($p < 0.005$) coordinated upregulation from DIV1 to DIV14 (Figure 3A), following the expression profile of most synaptic

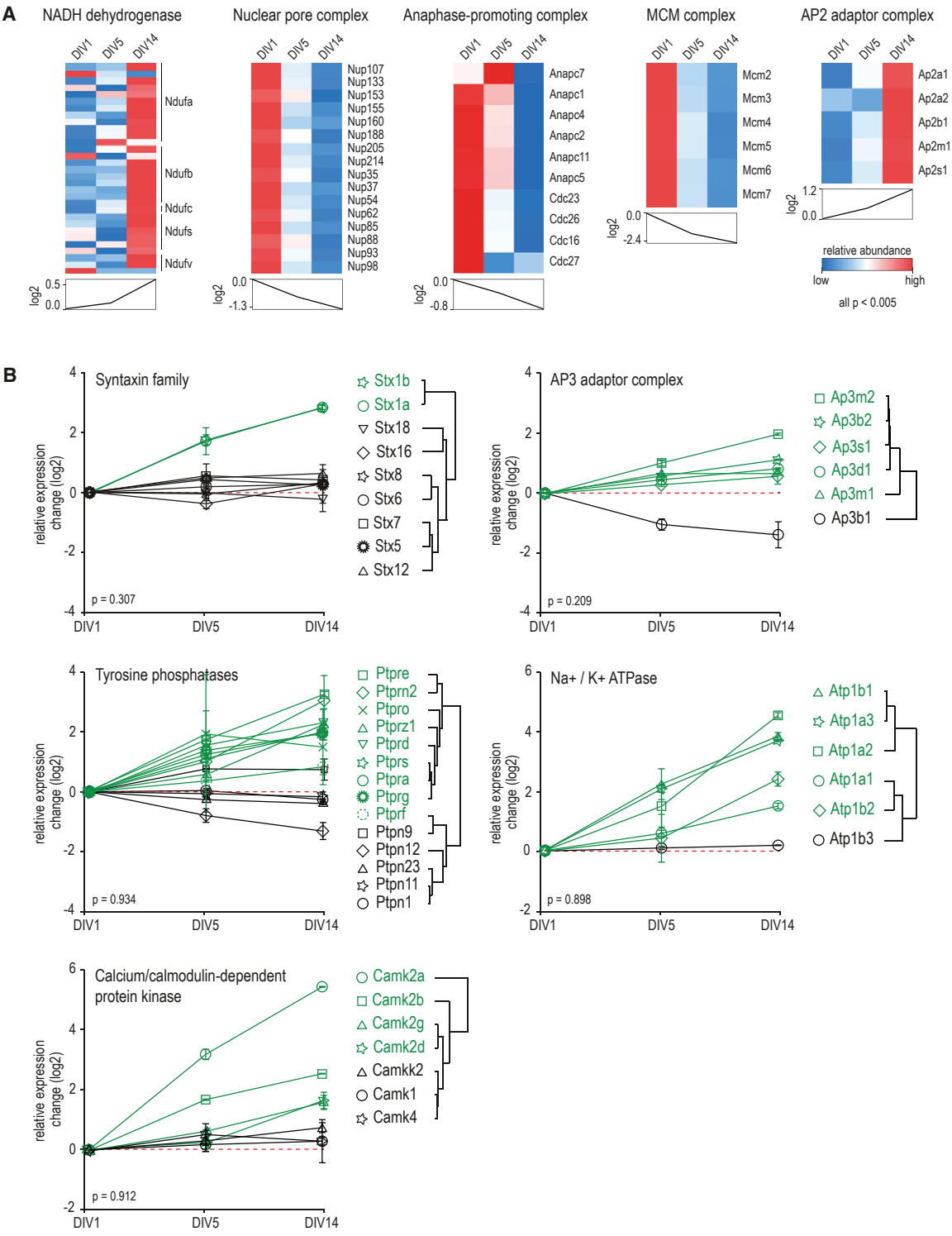

Figure 3. Significance Analysis of Protein Expression Profile Similarities for Proteins within Families or Complexes

(A) Examples of tight co-regulation of proteins that are part of larger protein complexes during neuronal development (all ps < 0.001). A complete list is given in Table S3.

(B) The same analysis reveals proteins within complexes or families that undergo divergent expression during differentiation. Hierarchical clustering further differentiates divergent protein expression. Error bars represent SD.

See also Figure S3B and Table S3.

proteins (cluster 2; Figure 2A). Strikingly, this does not hold for the AP3 complex ($p = 0.209$), where one isoform of the Ap3b subunit (Ap3b1) diverges from the common expression profile of the other complex proteins, including the neuron-specific isoform Ap3b2 (Figure 3B), implying functional regulation of the complex activity by Ap3b. It has recently been shown that neuronal AP3 complexes are assembled by one of the two Ap3b isoforms, regulating distinct vesicular sorting processes (Seong et al., 2005). Neuron-specific Ap3b2-containing AP3 mediates cargo sorting preferentially into synaptic vesicles, while ubiquitous Ap3b1-containing AP3 more likely promotes cargo delivery toward the lysosomes (Newell-Litwa et al., 2009). Moreover, neuronal AP3 was shown to be 4-fold more abundant in axons and dendrites than ubiquitous AP3 (Seong et al., 2005). Together, this substantiates our data across developmental stages 2–3 to 5, which are accompanied with dendrite formation, synaptogenesis, and maturation.

The richness of the neuron-specific proteome allowed us to further explore expression profiles of several other protein families. We observed distinct regulation of members of the tyrosine-protein phosphatase family, where receptor-type tyrosine phosphatases (Ptpr) undergo upregulation during neuronal differentiation, whereas most non-receptor-type tyrosine phosphatases (Ptpn) showed no expression changes (Figure 3B; Figure S3B). Hierarchical clustering further supports this observation by clearly separating the two subclasses. Ptps are important in signal transduction via a highly coordinated interplay with kinases (Tonks, 2013), and both classes are involved in cell-adhesion processes. Upregulation of the receptor-type Ptps implies an increased demand for cell-adhesion molecules in the course of dendrite outgrowth and synapse formation.

Similar observations were made for members of proteins from the Atp1- and Ca^{2+}/calmodulin-dependent protein kinase families. The main function of the Na/K-ATPase complex in neurons is to maintain the resting potential by using large amounts of the total cellular ATP supply. Interestingly, we observed that expression levels of Atp1b3 remain unchanged during neuronal differentiation, whereas all other subunits undergo upregulation, indicating a potential functional regulation through a stoichiometric change of the complex (Figure 3B; Figure S3B) (Ori et al., 2016). The ratio between the α and β subunit is 1:1 during assembly in the ER; however, the degradation rate of β subunits is known to be significantly higher. Moreover, each β isoform confers a different ATPase activity; thus, a change in stoichiometry indicates a potential cellular mechanism to regulate pump activity according to changes in Na^+ or K^+ concentrations, allowing maintenance of the resting potential or adjustment for changes in cell volume during neuronal differentiation. For the Ca^{2+}/calmodulin-dependent protein kinase family, we observed that Camk2 proteins, overall, upregulated during neuronal differentiation, whereas expression levels of the members of the Camk cascade (Camkk, Camk1, and Camk4) remained unchanged (Figure 3B; Figure S3B). The various Cam kinases differ in their subcellular localization. Camk2 predominantly localizes in dendrites, whereas Camkk and Camk1 are ubiquitous cytoplasmic proteins, and Camk4 is nuclear (Wayman et al., 2008). Camkk phosphorylates and activates Camk1 and Camk4, which act on further downstream targets in the MEK/Erk (mitogen-activated protein kinase/extracellular-signal-related kinase) pathway (Camk1) or modulate CREB (cAMP response element-binding protein)-mediated transcription (Camk4) (Wayman et al., 2008). In contrast, Camk2 is one of the major constituents of the post-synaptic density (PSD) and is a key player in mediating Ca^{2+}-influx-triggered signal transduction, modulation of synaptic plasticity, and induction of long-term potentiation. Notably, Camk2a is the most upregulated protein in our dataset. Our data clearly show an increased demand for PSD-localized Camk2 in growing and developing neurons.

Synaptic and Cell-Adhesion Protein Profiling during Neuronal Development

Next, we assessed the proteome dynamics during synaptogenesis, a key event in neuronal development that requires the coordinated assembly of a highly connected protein network that includes scaffolding proteins, receptors, and their downstream targets, signaling molecules, and cell-adhesion proteins. In our hippocampal neuron cultures, dividing non-neuronal cells are mostly represented by astrocytes. They expand after DIV5 (Figure S4A), thus promoting synapse formation and transmission. Indeed, synapse formation during the neuronal development of hippocampal neurons in culture occurs from stage 4 (DIV5) to stage 5 (DIV14) (Figure 4A). Interestingly, the majority of all differentially expressed synaptic proteins are allocated to cluster 2 (Table S4), which corresponds to a steady increase in relative protein levels from DIV1 to DIV14 (Figure 2A). This cluster includes important presynaptic proteins involved in vesicle trafficking (Syp and Syt1), cytoskeleton organization and protein anchoring (Cask, Pclo, Bsn), and neurotransmitter release (Syn1, Vamp2, Snap25, Sv2a, and Sv2b) (Figure 4C). Prominent members of the upregulated postsynaptic proteins are scaffold and anchoring proteins (Shank2, Psd95, Grip1, Homer1), and several glutamate and GABA receptors (Figure 4D; Figure S4B). To validate our quantitative proteomics data, we additionally plotted the relative expression of several proteins where we do not expect large changes (Figure 4F) and confirmed expression of several depicted proteins by western blot analysis (Figures 4G–4I) of lysates from the corresponding time points. These results were paralleled by immunoblotting of embryonic and adult rat hippocampal tissue, Hip.(E) and Hip.(A), respectively (Figure 4G), substantiating the observation of higher expression levels at later developmental stages. Presynaptic markers such as Bassoon (Bsn) and Synaptophysin (Syp) (Figure 4C) are known to accumulate at new synapses before postsynaptic proteins such as Psd95 (Friedman et al., 2000; Okabe et al., 2001). This is supported by our data, which show a later expression increase of Psd95 (Figure 4D). However, for the majority of postsynaptic proteins, we do not observe a timely delayed expression increase, which is also evident from hierarchical clustering analysis of all synaptic proteins (Figure S4D). This is likely because the temporal resolution of this study is limited by the experimental design. Nevertheless, our dataset demonstrates the substantial upregulation of many synaptic proteins already at early developmental stages, long before synaptogenesis takes place. Similar expression profiles are observed for subunits of various neurotransmitter receptors and voltage-gated ion channels (Figures S4B and S4C).

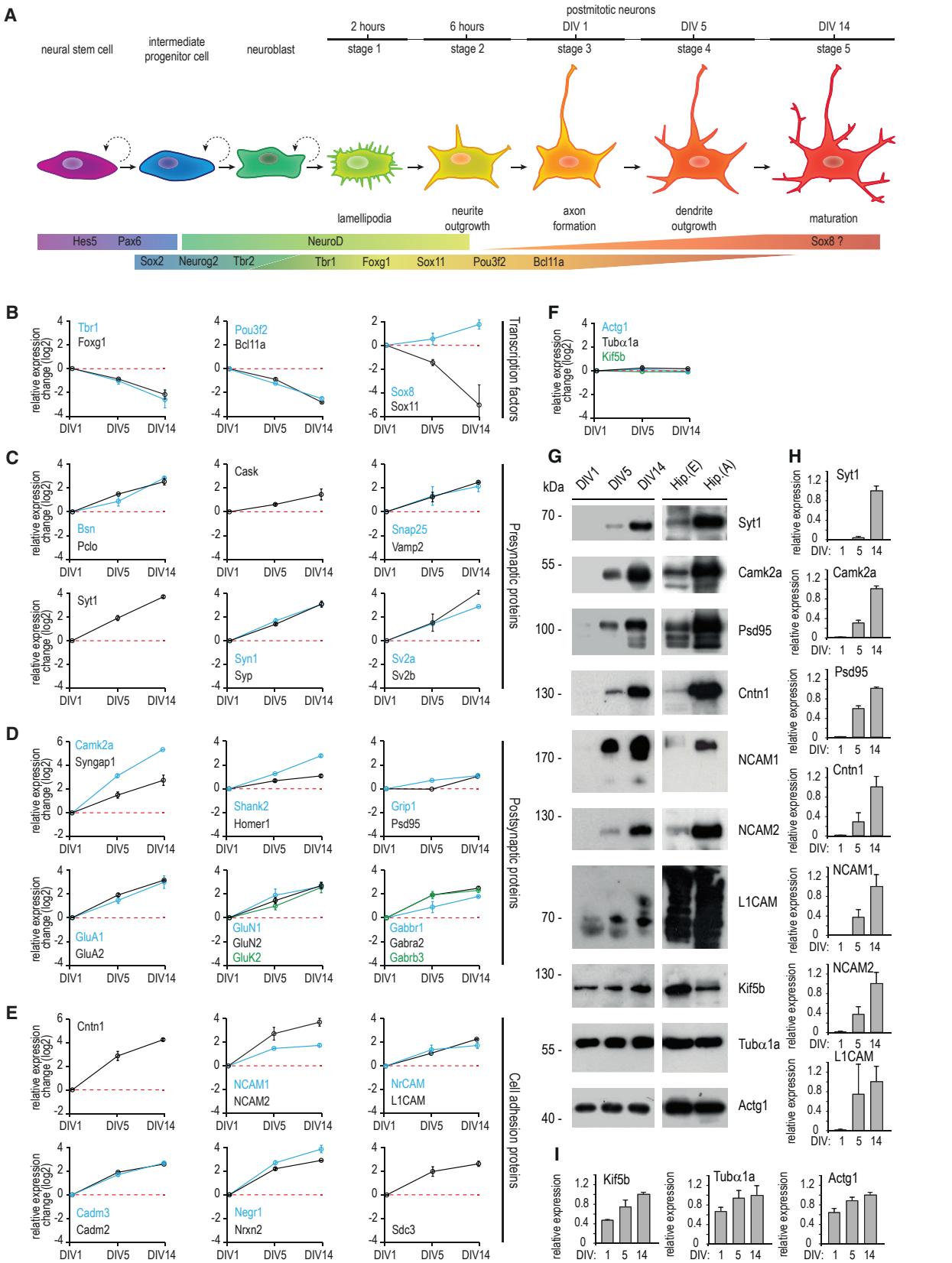

(legend on next page)

Cell-adhesion molecules are another important class of proteins with a key role in neuronal development. They mediate axon pathfinding and axon-dendrite contact formation, and they further modulate dendritic spine morphology and synaptic plasticity. In total, 82 cell-adhesion proteins were quantified in our dataset (Table S5), including Cntn1, NrCAM, Nrxn2, NCAM1, and NCAM2 (Figure 4E). Interestingly, 24 of these are allocated to cluster 3 (Figure 2A), highlighting that their major expression increase proceeds during the transition from stage 2–3 to stage 4, indicating an important role in dendrite formation. Neural cell-adhesion molecule 1 (NCAM1) is a prominent member of the cell-adhesion proteins that share the expression profile of cluster 3 (Figure 2A).

NCAM1 Is Highly Enriched in Dendritic Growth Cones

NCAM1 belongs to the immunoglobulin-like family of cell-adhesion molecules and is one of the most abundant neuronal adhesion proteins (Sharma et al., 2015). NCAM1 expresses in three main isoforms produced by alternative splicing of the NCAM1 gene. Two of the isoforms (NCAM140 and NCAM180) are transmembrane proteins, while NCAM120 is glycosylphosphatidylinositol (GPI) anchored (Figure 5A). We first analyzed by western blot isotype-specific protein expression levels in cultured rat hippocampal neurons extracts from DIV2 to DIV21 (Figure 5B). In agreement with previous observations, NCAM180 is the main isoform expressed in neurons (Noble et al., 1985). Quantification revealed that NCAM180 shows two main peaks of protein expression at DIV5 and DIV16 (Figure 5C), confirming our quantitative MS data and indicating that, in addition to its well-known role in synaptic plasticity (Doherty et al., 1995), NCAM1 may be important at earlier stages of neuronal development (DIV5).

To further investigate NCAM1 distribution in developing neurons (DIV1–DIV14), we performed triple-labeling immunofluorescence experiments using a NCAM1-specific antibody, the dendritic microtubule marker MAP2, and the F-actin marker phalloidin (Figure 5D). As reported previously, NCAM1 showed some staining in stage 2–3 cells (DIV1), which was mainly present in the axonal growth cones. Interestingly, at DIV4–DIV5, many neurons displayed strong accumulation of NCAM1 in dendritic growth cones. Here, NCAM1-rich dendritic growth cones are positive for F-actin but not for the microtubule marker MAP2, which is more restricted to the dendritic shaft (Figure 5E). Dendritic NCAM1 accumulations are present in approximately 40% of the neurons counted at DIV4, and during later stages (DIV6–DIV8), it gradually disappears (Figure 5F). At later developmental stages, NCAM1 was found diffusely distributed over the dendritic plasma membrane. Similar results were obtained with the mouse primary hippocampal culture, although here, NCAM1 was already localized in dendrites at DIV3 (Figure S5).

NCAM1 Is Required for Both Axonal and Dendritic Outgrowth and Branching

Since NCAM1 accumulates in dendritic growth cones, we further investigated the role of NCAM1 during dendritic development. Therefore, three specific short hairpin RNA (shRNA) sequences were designed and generated, based on the NCAM180 mRNA rat sequence, to perform knockdown experiments. All three shRNAs (shRNA_NCAM1#1, shRNA_NCAM1#2, and shRNA_NCAM1#3) reduced protein levels by ~80%, as revealed from both western blot analysis and immunostaining (Figures 6A–6C; Figure S6). We next examined the effect of NCAM1 knockdown on outgrowth of axon and dendrites (Figure 6D). Quantification revealed that both the length of the axon (Figure 6E) and length of the dendrites (Figure 6F) were significantly reduced compared to that of control neurons. The observed reduction of axon length in NCAM1-depleted neurons is consistent with that reported in previous works (Pollerberg et al., 2013). Apart from the axonal phenotype, NCAM1 depletion in young neurons also caused a marked reduction in dendrite development. Quantification indicated that knockdown of NCAM1 using three different shRNAs reduces the length of primary dendrites, total dendrites, and dendritic branches by 40% compared to control neurons (Figure 6F).

Actin Stabilization Rescues NCAM1 Knockdown Phenotype

To investigate the mechanism by which NCAM1 influences dendritic development, we searched for NCAM180-binding partners in neurons and used the other two isoforms as controls. The GFP-tagged NCAM1 isoforms were expressed in neurons to check their proper localization and their correct insertion in the cell membranes (Figures S7A and S7B). Subsequently, constructs of all three GFP-NCAM1 isoforms and GFP (as control) were transiently expressed in HEK293 cells; GFP proteins were isolated with GFP beads and incubated with either young (postnatal day 5; P5) or adult rat brain extracts, and then co-isolated proteins were analyzed in an affinity purification (AP)-MS experiment. To identify true NCAM1-binding partners (in adult or young brains), we used the "Significance Analysis of INTeractome (SAINT)" for probabilistic scoring of our AP-MS data (Choi et al., 2011). Among the entire list of putative interacting proteins identified (Table S6), only those with a SAINT probability > 0.75 (false discovery rate [FDR] = 0.1) were considered as true interactors and were then represented as spheres of different size and color according to their relative abundance and obtained p value, respectively (Figure 7A). Interestingly, several members of actin-binding, -stabilizing and/or -polymerizing proteins such as spectrin (Spt) and myosin (Myo/Myh); actin-related

Figure 4. Protein Expression Changes during Neuronal Differentiation

(A) Schematic overview of neurogenesis, illustrating the distinct developmental stages and representative transcription factors involved.

(B) Expression profiles for representative transcription factors including the most downregulated protein in this dataset, Sox11.

(C–F) Expression profiles of selected presynaptic proteins (C), postsynaptic proteins (D), cell-adhesion proteins (E) and proteins with no relative expression change over the developmental stages (F).

(G) Change in the protein expression during neuronal development shown by western blot analysis from cultured hippocampal neurons, embryonic tissue (Hip.(E)), and adult brain tissue (Hip.(A)).

(H and I) Graphs showing the quantifications of relative intensities of the western blot analysis in (G), shown in (H), and control proteins, shown in (I). n = 3 experiments per condition. Error bars indicate mean ± SEM.

In (B)–(F), error bars represent SD.

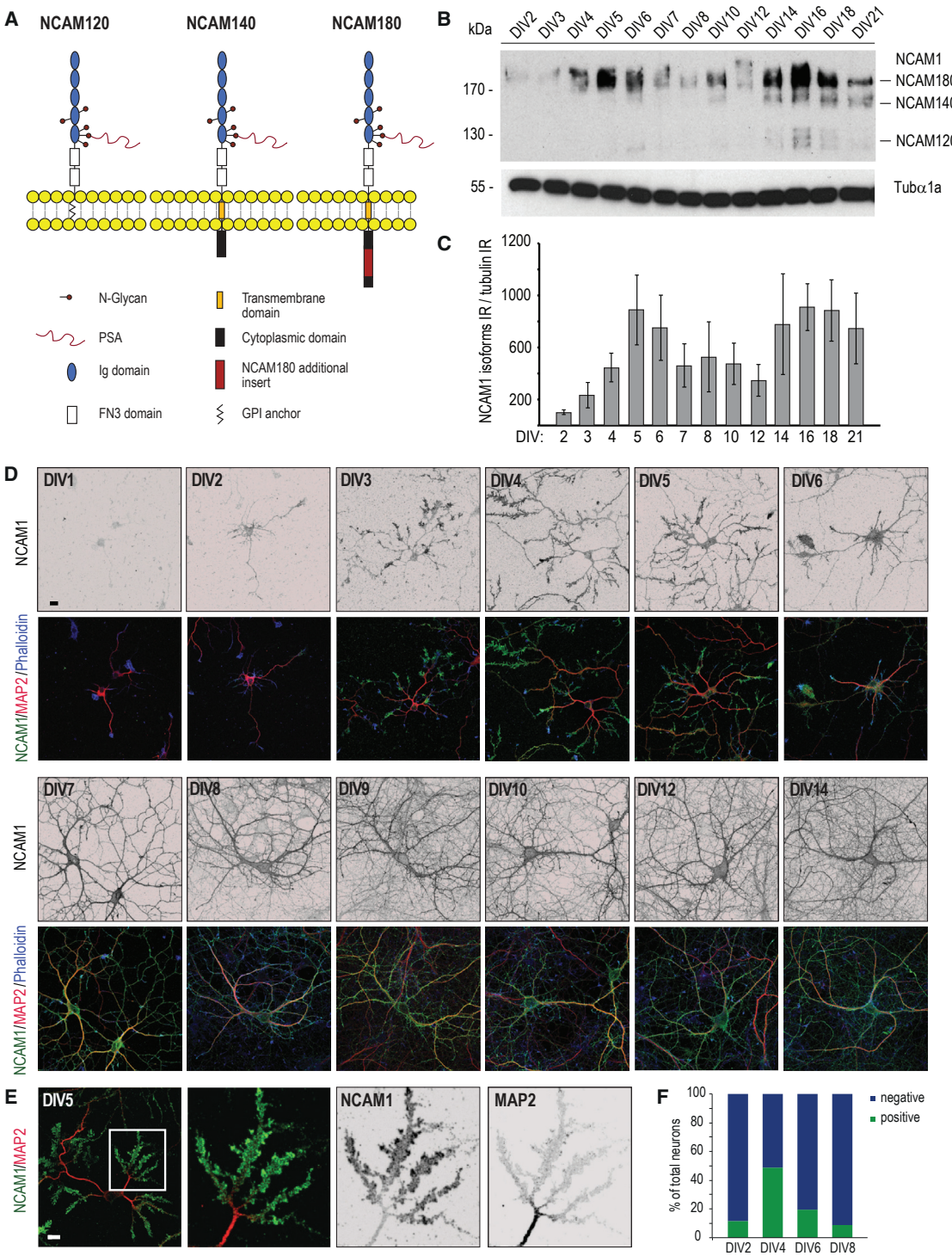

Figure 5. The Cell-Adhesion Molecule NCAM1 and Its Expression throughout Neuronal Development

(A) Schematic overview of the three main NCAM1 isoforms. Ig, immunoglobulin.

(B and C) Western blot analysis (B) and quantification (C) of developmental expression of NCAM1 in DIV2–DIV21 rat hippocampal neurons. Error bars indicate mean ± SEM.

(D) Representative images of rat hippocampal neurons from DIV1 to DIV14, stained for NCAM1 (green), MAP2 (red), and phalloidin (blue). Scale bar, 20 μm.

(E) Representative rat hippocampal neuron at DIV5 stained for NCAM1 (green) and MAP2 (red). Scale bar, 20 μm.

(F) Quantification of the percentage of neurons characterized by the NCAM1 dendritic staining shown in (D) and (E). n = 100 cells per DIV.

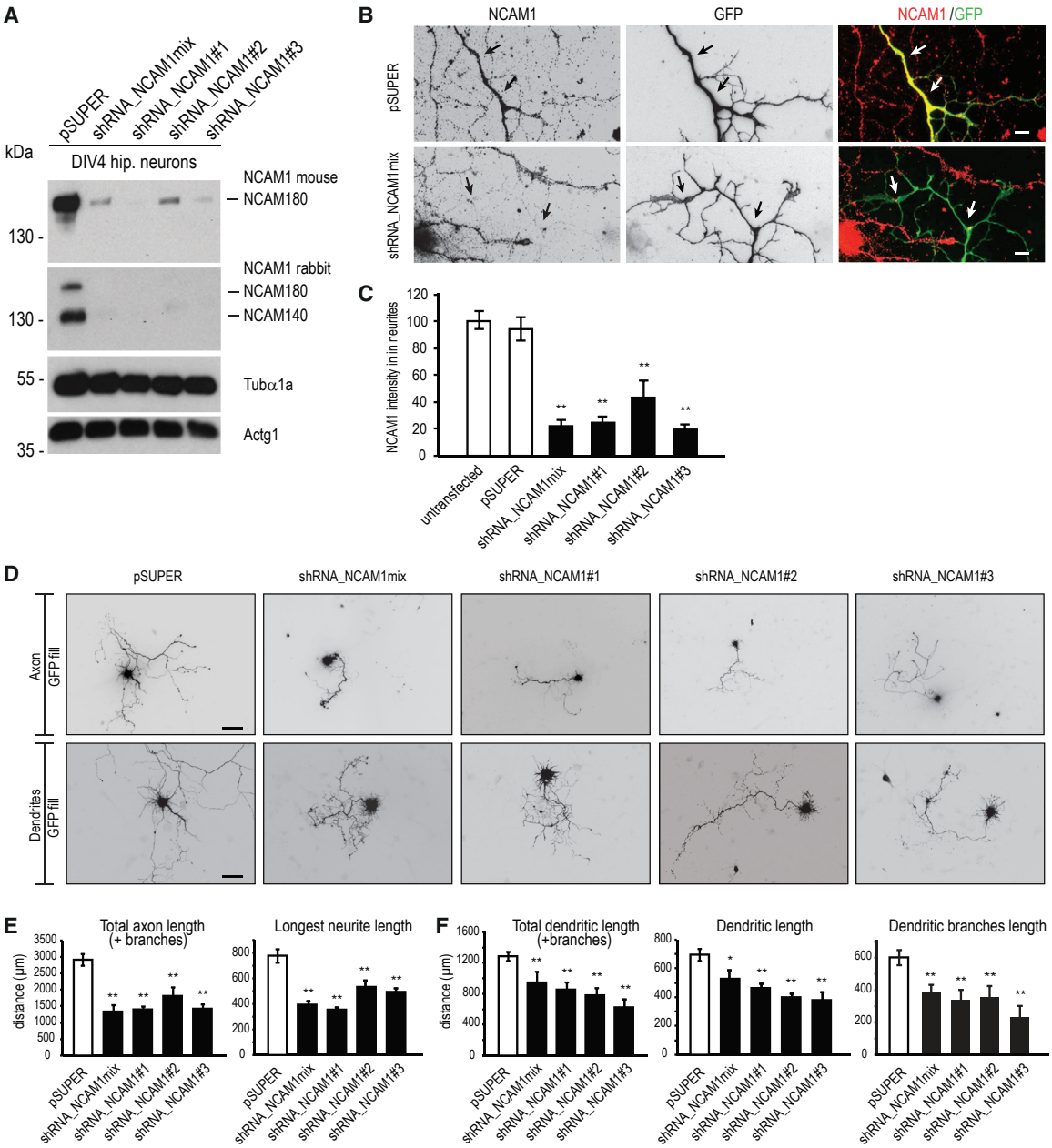

Figure 6. shRNA-Mediated Knockdown of NCAM1 in Neurons

(A) Knockdown of NCAM1 by indicated shRNA constructs and analyzed by western blot in DIV4 cortical neurons.

(B) Representative images of hippocampal neurons at DIV4 co-transfected with indicated constructs and stained with NCAM1 monoclonal antibody. Arrows indicate transfected neurites.

(C) Quantification of NCAM1 fluorescent-staining intensities in neurites of hippocampal neurons co-transfected at DIV4 with indicated constructs.

(D) Representative images of primary hippocampal neurons co-transfected with indicated constructs (DIV1–DIV7) to visualize axon (top) and dendrite (bottom) morphology.

(E and F) Quantification of axon (E) and dendrite (F) morphological parameters.

Error bars indicate mean ± SEM. *$p < 0.5$, t test; **$p < 0.01$, t test. Scale bars, 10 μm in (B), 100 μm for the top of (D), and 50 μm for the bottom of (D).

proteins (Arps), tropomyosins (Tpms); F-actin-capping proteins (Capzas); and actinins (Actn) are the main neuronal interactors of NCAM1, ubiquitously enriched in young brains and, to a lesser extent, in adult brains. The interaction between the NCAM140 and NCAM180 intracellular tails and actin-cytoskeleton-related proteins (Spt, α-Actn, and Tpm) has been already reported and characterized in previous studies (Pollerberg et al., 2013). In our AP-MS experiments, it is interesting to notice that the length of each NCAM1 isoform used as bait directly correlates with the relative abundance of each specific actin-binding protein

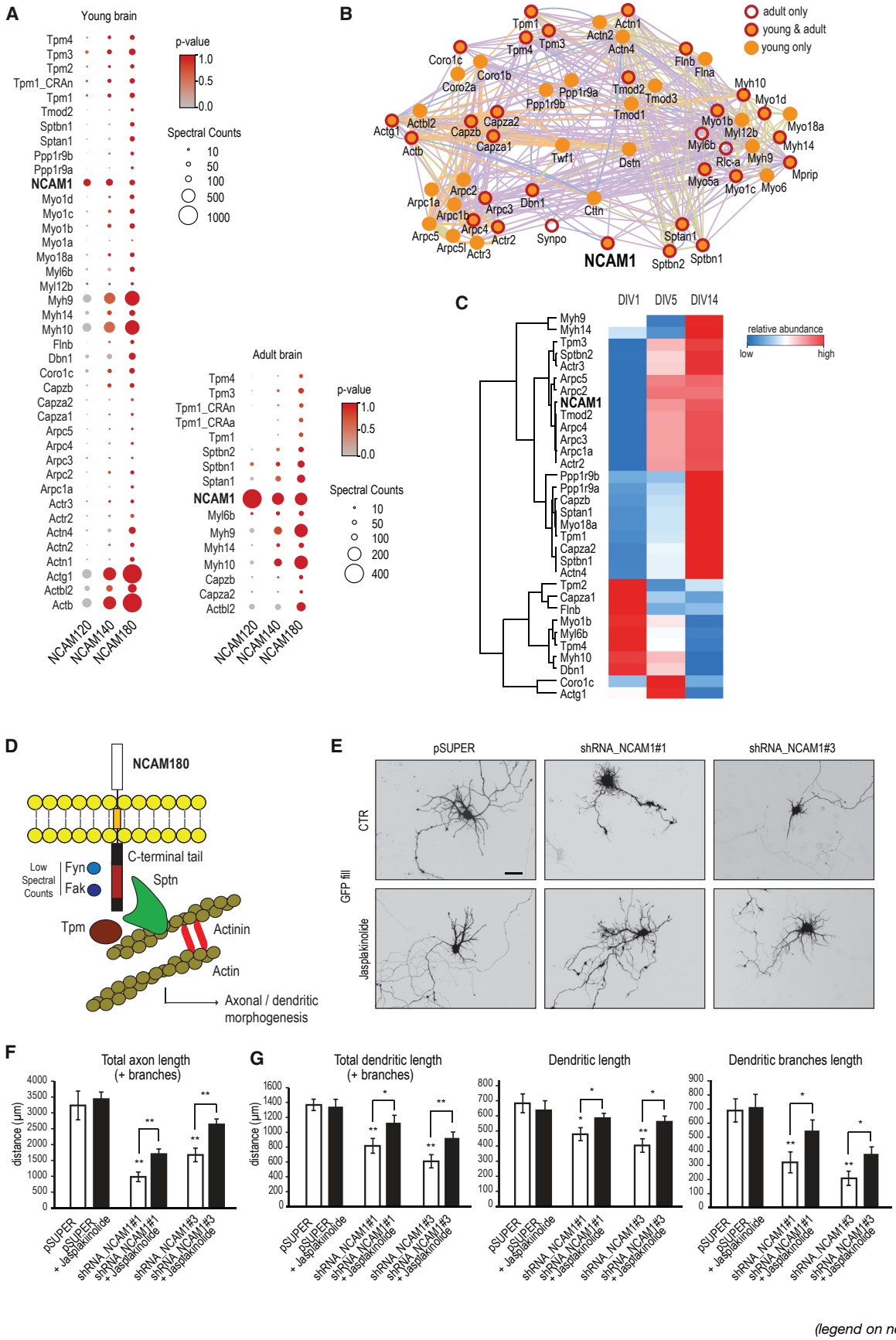

(legend on next page)

identified (as indicated by the amount of peptides and peptide-spectrum matches [PSMs] measured), thus corroborating the hypothesis that NCAM180 (with its longer C terminus) might be the main player involved in the regulation of actin dynamics in dendrites (Figure 7A; Table S6). By drawing a protein interaction network (Cytoscape, Genemania plugin), using as input the actin-binding proteins identified in the NCAM180 pull-down, it becomes evident how these proteins are tightly connected (Figure 7B). Similarly to NCAM1, most actin-interacting proteins are grouped in the earlier defined cluster 3 (Figure 2A) and upregulated at DIV5 (Figure 7C), suggesting that they may strongly cooperate in NCAM1 signaling.

To investigate the potential relationship between NCAM1 and the actin cytoskeleton (Figure 7D), we tested whether the dendritic phenotype caused by NCAM1 depletion can be reversed by jasplakinolide-forced F-actin stabilization. Jasplakinolide is a drug known to stabilize actin fibers and to facilitate actin polymerization. Thus, neurons were first transfected with the two most efficient NCAM1 shRNAs (ShRNA_NCAM1#1 and ShRNA_NCAM1#3), and 24 hr later, a low dose of jasplakinolide (10nM) was added to the growth medium for 6 days. The addition of jasplakinolide partially rescues the neuronal developmental defects caused by NCAM1 depletion, as demonstrated by the quantification of the axonal and dendritic parameters (Figures 7E–7G). Total dendritic length, primary dendrite length, and dendritic branch length were significantly increased in jasplakinolide-treated neurons compared to control neurons (Figure 7G). Together, the presented data indicate actin stabilization as a mechanism for NCAM1-mediated dendritic growth.

DISCUSSION

The in-depth analysis of neuronal proteins that are abundantly and differentially expressed during the well-defined stages of differentiation is a promising strategy for understanding neurodevelopment-regulated processes. We provide proof of concept by applying this strategy to identify and characterize the role of NCAM1 in dendritic outgrowth.

A Quantitative Map of Proteome Dynamics during Neuronal Differentiation

In neurons, like in all other cells, proteins are the main functional components, but how the proteomes differ in developing neurons is not known. To resolve the global neuronal proteome and to determine the basis for cellular differentiation, we performed a quantitative analysis of protein levels by combining triplex stable-isotope dimethyl labeling coupled to high-resolution LC-MS/MS of hippocampal neurons in culture. Here, we found that 1,793 proteins show more than 2-fold expression changes during the different developmental steps, indicating extensive remodeling of the neuron proteome during early differentiation. This analysis revealed six clusters of distinct expression profiles, with proteins upregulated during differentiation in clusters 1, 2, and 3 and proteins downregulated present in clusters 4, 5, and 6. We mainly focused our attention on cluster 3, which contains proteins whose expression levels are highly upregulated between stages 2–3 and stage 4 of in vitro neuronal development. According to GO classification, most of the proteins present in this cluster are transmembrane proteins that could play a role by modulating dendritic outgrowth and branching. It is interesting to notice that, during these stages of neuronal development, a very specific group of NCAM-adhesion molecules (NCAM1, NCAM2, NRCAM, and L1CAM) is characterized by exactly the same pattern of protein-level regulation (Figure 4E), suggesting that these proteins may act synergistically. On the other hand, pre- and postsynaptic proteins are highly represented in cluster 2, indicating that their expression levels increase throughout neuronal development. These data strongly support a model in which specific synaptic scaffolding proteins such as Bassoon, Piccolo (pre-synaptic proteins), Shank, and Camk2A (post-synaptic proteins) are expressed prior to synapse formation. The full datasets are available in Tables S1, S2, S3, S4, and S5.

NCAM1 Plays an Important Role in Dendritic Outgrowth

To demonstrate the strength of our resource, we focused on NCAM1 as a regulator for dendritic outgrowth. NCAM1 is best known for its role in axonal wiring through interactions with various ligands via its extracellular domain (Pollerberg et al., 2013). NCAM1 is unique among the adhesion molecules because it carries a polysialic acid (Togashi et al., 2009), which can be reversibly attached to extracellular domains, reducing its homophilic interactions and thereby controlling clustering and downstream signaling of NCAM1 (Pollerberg et al., 2013). The cytosolic part of the longer NCAM1 isoform (NCAM180) interacts with several cytoskeletal elements and signaling molecules. NCAM1 is reportedly involved in neurite outgrowth and axon pathfinding (Walsh and Doherty, 1997). For example, in mice lacking NCAM1, hippocampal axons show abnormal pathfinding (Cremer et al., 1997). Our data suggest that NCAM1 not

Figure 7. NCAM1 and Its Role in Actin Cytoskeleton Stabilization

(A) Selected candidates of putative NCAM1 interactors identified in young and adult rat brains by AP-MS experiments (see Table S6 for the complete list of proteins). SAINT probability cutoff > 0.75 corresponds to an average FDR of 0.1. The p values and spectral counts are graphically represented by colors and spheres, respectively.

(B) Network analysis on selected NCAM180-binding proteins linked to actin cytoskeleton. Edge color coding: blue, co-localization; orange, predicted interaction; green, shared protein domain; purple, co-expression.

(C) Heatmap and hierarchical clustering of the expression profiles of selected NCAM1-interacting proteins.

(D) Schematic representation of NCAM180 associated with actin-stabilizing proteins.

(E) Representative images of primary hippocampal neurons co-transfected with indicated constructs (DIV1–DIV7) and treated 24 hr later with DMSO or 10 nM jasplakinolide. Scale bar, 50 μm.

(F and G) Quantification of axon (F) and dendrite (G) morphological parameters.

Error bars indicate mean ± SEM. *p < 0.5, t test; **p < 0.01, t test.

See also Table S6.

only plays a role in axon outgrowth and guidance but is also required for proper dendritic outgrowth during first days of neuronal development. We speculate that NCAM180 is the specific isoform playing a role in dendrites based on the developmental expression pattern. Consistently, NCAM180 is strongly upregulated during dendrite outgrowth and highly enriched in dendritic growth cones. Interestingly, other NCAM family proteins have been reported to be involved in dendritic branching and morphology in *C. elegans* (Dong et al., 2013). It is likely that, similar to its role in axonal growth cones, NCAM1 at the tips of dendrites may sense various types of extrinsic signals, such as other CAMs or various diffusible factors that determine their general orientation and outgrowth (Pollerberg et al., 2013). The extracellular signals may come from crossing axons, dendrites from the same cell, and neighboring arbors and together regulate the immense complexity of dendrite morphology.

Actin Stabilization as a Mechanism for NCAM1-Mediated Dendritic Growth

Our AP-MS experiments revealed that NCAM180 interacts with several members of actin-binding, -stabilizing and/or -polymerizing proteins in young and adult brains. These data are consistent with the previously reported interactions between the NCAM1 intracellular tails and actin-related proteins (Büttner et al., 2003; Leshchyns'ka and Sytnyk, 2016). These observations suggest that NCAM1 can act as a scaffold for multiple cytoskeleton components and that multiple actin-binding proteins can amplify the interaction between NCAM1 with the actin cytoskeleton. However, it is also possible that these interactions do not occur simultaneously but are rather highly regulated in response to the extracellular signals (Leshchyns'ka and Sytnyk, 2016). Interestingly, inducing actin polymerization by jasplakinolide treatment partially rescues the dendritic phenotype of NCAM1 depletion. These results indicate that forced actin stabilization can compensate for the absence of NCAM1 and is one of the driving forces that act during dendrite morphogenesis. These data suggest a model in which NCAM1 stimulates dendritic arbor development by promoting actin filament stabilization at the dendritic growth cone.

In summary, the analysis of proteins differentially expressed at each specific stage of hippocampal neuron development constitutes a fundamental research tool that may be used in the future for a better understanding of any specific molecular mechanism involved in neurodevelopment. Our quantitative proteomics results give a comprehensive overview of protein abundances in time, thereby providing a unique database regarding protein expression patterns in cultured neurons. Furthermore, thanks to the recent technological advances in MS-based proteomics (tandem mass tags [TMTs] or iTRAQ isobaric mass tags would allow relative quantification of up to ten different time points), this analysis could also constitute an excellent starting point for other studies that aim to further complement our understanding of neuronal protein dynamics.

EXPERIMENTAL PROCEDURES

Animals

All experiments with animals were performed in compliance with the guidelines for the welfare of experimental animals issued by the Government of the Netherlands and were approved by the Animal Ethical Review Committee (DEC) of Utrecht University.

Expression Vectors, shRNA Constructs, and Antibodies

The NCAM120, NCAM140, and NCAM180 constructs were kindly provided by Dr. Landmesser. The following NCAM1 shRNAs were designed and used in this study: NCAM1#1 (5′-GGATCTCATCTGGACTTTG), NCAM1#2 (5′-GATCTTCCAGAAGCTCATG), and NCAM1#3 (CGTTGGAGAGTC CAAATTC) targeting rat NCAM1 mRNA (NM_031521.1). NCAM1 mouse (Millipore) and NCAM1 rabbit (Proteintech) antibodies were used for western blot and immunocytochemistry experiments. For further details, see Supplemental Experimental Procedures.

Primary Hippocampal Neuron Cultures

Primary hippocampal and cortical cultures were isolated from embryonic day 18 (E18) rat brains. Cells were plated on coverslips coated with poly-L-lysine (30 μg/mL) and laminin (2 μg/mL) at a density of 100,000 per well. Hippocampal neurons were transfected at DIV1 using Lipofectamine 2000 (Invitrogen). Cortical neurons were transfected using the Amaxa Rat Neuron Nucleofector Kit (Lonza). For further details, see Supplemental Experimental Procedures.

Sample Preparation, Peptide Fractionation, MS, and Data Analysis

The MS methods and any associated references are available in the online version of this paper.

Statistical Methods

Analysis of significance of proteins changing between developmental stages was carried out using the significance analysis of microarrays (SAM). Clustering was performed using unsupervised fuzzy clustering. Gene Ontology enrichment analyses were performed using a Fisher's exact test. Co-regulation of proteins within complexes or families was assessed using the R package protein profiles. coIP data were analyzed using the SAINT. For morphometric analyses of hippocampal neurons, statistical significance was determined using Student's t test assuming a two-tailed variation. The graphs represent mean ± SEM. For further details, see Supplemental Experimental Procedures.

ACCESSION NUMBERS

The accession number for the mass spectrometry proteomics data reported in this paper is PRIDE: PXD005031 (Vizcaíno et al., 2016).

SUPPLEMENTAL INFORMATION

Supplemental Information includes Supplemental Experimental Procedures, seven figures, and six tables and can be found with this article online at http://dx.doi.org/10.1016/j.celrep.2017.01.025.

AUTHOR CONTRIBUTIONS

C.K.F. designed and performed the quantitative proteomics experiments and analyzed the data; Q.L. conducted proteomics sample preparation; M.M. and R.S. designed and performed immunohistochemistry and biochemical experiments and analyzed the data. R.S. and V.G. performed AP/MS experiments, and C.K.F. and R.S. analyzed the results. S.M. and A.J.R.H. supervised the quantitative proteomics experimental setup and the mass spectrometry data. The figures were designed and assembled by C.K.F., M.M., R.S., A.F.M.A., and C.C.H. The manuscript was written by C.K.F., M.M., R.S., A.F.M.A., and C.C.H., with input from A.J.R.H.; A.F.M.A. and C.C.H. supervised the project and coordinated the study.

ACKNOWLEDGMENTS

We thank Dr. L.T. Landmesser for sharing the NCAM120, NCAM140, and NCAM180 constructs. This work was supported by the Netherlands Organization for Scientific Research (NWO) (NWO-ALW-VICI 865.10.010 to

C.C.H. and NWO-CW-VIDI 723.012.102 to A.F.M.A.) and Proteins@Work, a program of the NWO, as part of the National Roadmap Large-Scale Research Facilities of the Netherlands (project number 184.032.201); the Foundation for Fundamental Research on Matter (FOM programme number 137; to C.C.H.), which is part of the NWO; the Netherlands Organization for Health Research and Development (ZonMW-TOP 91213017 and 91215084; to C.C.H.); the European Research Council (ERC) (ERC Consolidator grant 617050 to C.C.H.); Marie-Curie Actions (FP7-MC-IEF 300814; to M.M.), and the DFG Emmy-Noether Programm (MI 1923/1-1 to M.M.).

Received: October 31, 2016
Revised: January 8, 2017
Accepted: January 11, 2017
Published: February 7, 2017

REFERENCES

Boehm, M., and Bonifacino, J.S. (2001). Adaptins: the final recount. Mol. Biol. Cell *12*, 2907–2920.

Boersema, P.J., Raijmakers, R., Lemeer, S., Mohammed, S., and Heck, A.J.R. (2009). Multiplex peptide stable isotope dimethyl labeling for quantitative proteomics. Nat. Protoc. *4*, 484–494.

Büttner, B., Kannicht, C., Reutter, W., and Horstkorte, R. (2003). The neural cell adhesion molecule is associated with major components of the cytoskeleton. Biochem. Biophys. Res. Commun. *310*, 967–971.

Choi, H., Larsen, B., Lin, Z.Y., Breitkreutz, A., Mellacheruvu, D., Fermin, D., Qin, Z.S., Tyers, M., Gingras, A.C., and Nesvizhskii, A.I. (2011). SAINT: probabilistic scoring of affinity purification-mass spectrometry data. Nat. Methods *8*, 70–73.

Cremer, H., Chazal, G., Goridis, C., and Represa, A. (1997). NCAM is essential for axonal growth and fasciculation in the hippocampus. Mol. Cell. Neurosci. *8*, 323–335.

Dabrowski, M., Aerts, S., Van Hummelen, P., Craessaerts, K., De Moor, B., Annaert, W., Moreau, Y., and De Strooper, B. (2003). Gene profiling of hippocampal neuronal culture. J. Neurochem. *85*, 1279–1288.

DeBoer, E.M., Kraushar, M.L., Hart, R.P., and Rasin, M.R. (2013). Post-transcriptional regulatory elements and spatiotemporal specification of neocortical stem cells and projection neurons. Neuroscience *248*, 499–528.

Doherty, P., Fazeli, M.S., and Walsh, F.S. (1995). The neural cell adhesion molecule and synaptic plasticity. J. Neurobiol. *26*, 437–446.

Dominguez, M.H., Ayoub, A.E., and Rakic, P. (2013). POU-III transcription factors (Brn1, Brn2, and Oct6) influence neurogenesis, molecular identity, and migratory destination of upper-layer cells of the cerebral cortex. Cereb. Cortex *23*, 2632–2643.

Dong, X., Liu, O.W., Howell, A.S., and Shen, K. (2013). An extracellular adhesion molecule complex patterns dendritic branching and morphogenesis. Cell *155*, 296–307.

Dotti, C.G., Sullivan, C.A., and Banker, G.A. (1988). The establishment of polarity by hippocampal neurons in culture. J. Neurosci. *8*, 1454–1468.

Friedman, H.V., Bresler, T., Garner, C.C., and Ziv, N.E. (2000). Assembly of new individual excitatory synapses: time course and temporal order of synaptic molecule recruitment. Neuron *27*, 57–69.

Haslinger, A., Schwarz, T.J., Covic, M., and Lie, D.C. (2009). Expression of Sox11 in adult neurogenic niches suggests a stage-specific role in adult neurogenesis. Eur. J. Neurosci. *29*, 2103–2114.

Hevner, R.F., Hodge, R.D., Daza, R.A.M., and Englund, C. (2006). Transcription factors in glutamatergic neurogenesis: conserved programs in neocortex, cerebellum, and adult hippocampus. Neurosci. Res. *55*, 223–233.

Hsieh, J. (2012). Orchestrating transcriptional control of adult neurogenesis. Genes Dev. *26*, 1010–1021.

Kristensen, A.R., Gsponer, J., and Foster, L.J. (2013). Protein synthesis rate is the predominant regulator of protein expression during differentiation. Mol. Syst. Biol. *9*, 689.

Kuo, T.Y., Hong, C.J., and Hsueh, Y.P. (2009). Bcl11A/CTIP1 regulates expression of DCC and MAP1b in control of axon branching and dendrite outgrowth. Mol. Cell. Neurosci. *42*, 195–207.

Leshchyns'ka, I., and Sytnyk, V. (2016). Reciprocal interactions between cell adhesion molecules of the immunoglobulin superfamily and the cytoskeleton in neurons. Front. Cell Dev. Biol. *4*, 9.

Licatalosi, D.D., Yano, M., Fak, J.J., Mele, A., Grabinski, S.E., Zhang, C., and Darnell, R.B. (2012). Ptbp2 represses adult-specific splicing to regulate the generation of neuronal precursors in the embryonic brain. Genes Dev. *26*, 1626–1642.

Low, T.Y., van Heesch, S., van den Toorn, H., Giansanti, P., Cristobal, A., Toonen, P., Schafer, S., Hübner, N., van Breukelen, B., Mohammed, S., et al. (2013). Quantitative and qualitative proteome characteristics extracted from in-depth integrated genomics and proteomics analysis. Cell Rep. *5*, 1469–1478.

Loya, C.M., Van Vactor, D., and Fulga, T.A. (2010). Understanding neuronal connectivity through the post-transcriptional toolkit. Genes Dev. *24*, 625–635.

Méndez-Gómez, H.R., Vergaño-Vera, E., Abad, J.L., Bulfone, A., Moratalla, R., de Pablo, F., and Vicario-Abejón, C. (2011). The T-box brain 1 (Tbr1) transcription factor inhibits astrocyte formation in the olfactory bulb and regulates neural stem cell fate. Mol. Cell. Neurosci. *46*, 108–121.

Mody, M., Cao, Y., Cui, Z., Tay, K.Y., Shyong, A., Shimizu, E., Pham, K., Schultz, P., Welsh, D., and Tsien, J.Z. (2001). Genome-wide gene expression profiles of the developing mouse hippocampus. Proc. Natl. Acad. Sci. USA *98*, 8862–8867.

Newell-Litwa, K., Salazar, G., Smith, Y., and Faundez, V. (2009). Roles of BLOC-1 and adaptor protein-3 complexes in cargo sorting to synaptic vesicles. Mol. Biol. Cell *20*, 1441–1453.

Noble, M., Albrechtsen, M., Møller, C., Lyles, J., Bock, E., Goridis, C., Watanabe, M., and Rutishauser, U. (1985). Glial cells express N-CAM/D2-CAM-like polypeptides in vitro. Nature *316*, 725–728.

Okabe, S., Miwa, A., and Okado, H. (2001). Spine formation and correlated assembly of presynaptic and postsynaptic molecules. J. Neurosci. *21*, 6105–6114.

Ori, A., Iskar, M., Buczak, K., Kastritis, P., Parca, L., Andrés-Pons, A., Singer, S., Bork, P., and Beck, M. (2016). Spatiotemporal variation of mammalian protein complex stoichiometries. Genome Biol. *17*, 47.

Pollerberg, G.E., Thelen, K., Theiss, M.O., and Hochlehnert, B.C. (2013). The role of cell adhesion molecules for navigating axons: density matters. Mech. Dev. *130*, 359–372.

Sawicka, K., Bushell, M., Spriggs, K.A., and Willis, A.E. (2008). Polypyrimidine-tract-binding protein: a multifunctional RNA-binding protein. Biochem. Soc. Trans. *36*, 641–647.

Seong, E., Wainer, B.H., Hughes, E.D., Saunders, T.L., Burmeister, M., and Faundez, V. (2005). Genetic analysis of the neuronal and ubiquitous AP-3 adaptor complexes reveals divergent functions in brain. Mol. Biol. Cell *16*, 128–140.

Sharma, K., Schmitt, S., Bergner, C.G., Tyanova, S., Kannaiyan, N., Manrique-Hoyos, N., Kongi, K., Cantuti, L., Hanisch, U.K., Philips, M.A., et al. (2015). Cell type- and brain region-resolved mouse brain proteome. Nat. Neurosci. *18*, 1819–1831.

Stolt, C.C., Lommes, P., Friedrich, R.P., and Wegner, M. (2004). Transcription factors Sox8 and Sox10 perform non-equivalent roles during oligodendrocyte development despite functional redundancy. Development *131*, 2349–2358.

Togashi, H., Sakisaka, T., and Takai, Y. (2009). Cell adhesion molecules in the central nervous system. Cell Adhes. Migr. *3*, 29–35.

Tonks, N.K. (2013). Protein tyrosine phosphatases–from housekeeping enzymes to master regulators of signal transduction. FEBS J. *280*, 346–378.

van Spronsen, M., van Battum, E.Y., Kuijpers, M., Vangoor, V.R., Rietman, M.L., Pothof, J., Gumy, L.F., van Ijcken, W.F.J., Akhmanova, A., Pasterkamp, R.J., and Hoogenraad, C.C. (2013). Developmental and activity-dependent

miRNA expression profiling in primary hippocampal neuron cultures. PLoS ONE *8*, e74907.

Vizcaíno, J.A., Csordas, A., del-Toro, N., Dianes, J.A., Griss, J., Lavidas, I., Mayer, G., Perez-Riverol, Y., Reisinger, F., Ternent, T., et al. (2016). 2016 update of the PRIDE database and its related tools. Nucleic Acids Res. *44* (*D1*), D447–D456.

Walsh, F.S., and Doherty, P. (1997). Neural cell adhesion molecules of the immunoglobulin superfamily: role in axon growth and guidance. Annu. Rev. Cell Dev. Biol. *13*, 425–456.

Wayman, G.A., Lee, Y.S., Tokumitsu, H., Silva, A.J., and Soderling, T.R. (2008). Calmodulin-kinases: modulators of neuronal development and plasticity. Neuron *59*, 914–931.

White, M.K., Johnson, E.M., and Khalili, K. (2009). Multiple roles for Puralpha in cellular and viral regulation. Cell Cycle *8*, 1–7.

Zhang, J., and Herrup, K. (2011). Nucleocytoplasmic Cdk5 is involved in neuronal cell cycle and death in post-mitotic neurons. Cell Cycle *10*, 1208–1214.

Cell Reports, Volume *18*

Supplemental Information

Quantitative Map of Proteome Dynamics during Neuronal Differentiation

Christian K. Frese, Marina Mikhaylova, Riccardo Stucchi, Violette Gautier, Qingyang Liu, Shabaz Mohammed, Albert J.R. Heck, A.F. Maarten Altelaar, and Casper C. Hoogenraad

SUPPLEMENTAL TABLES

Table S1 – Related to Figure 1. All proteins quantified in the analysis

Contains the complete proteomics data set containing all identified proteins. ID = unique identifier for each protein; Uniprot = Uniprot accession code; gene name = corresponding gene name; Description = Protein name/description derived from *.fasta database; Σ# Unique Peptides = sum of unique peptides per protein; repl.1 DIV5/DIV1 = log2 fold change between DIV5 and DIV1 from replicate 1; repl.2 DIV5/DIV1 = log2 fold change between DIV5 and DIV1 from replicate 2; repl.1 DIV14/DIV5 = log2 fold change between DIV14 and DIV5 from replicate 1; repl.2 DIV14/DIV5 = log2 fold change between DIV14 and DIV5 from replicate 2; quantified = if a protein was quantified at all time points and in both replicates it is flagged "all"; average log2 DIV5/DIV1 = the average log2 fold-change between DIV5 and DIV1; average log2 DIV14/DIV5 = the average log2 fold-change between DIV14 and DIV5; SAM q-value [%] = q-value derived from statistical analysis of global proteome changes (lower values correspond to higher statistical significance); GProX cluster = cluster derived from fuzzy clustering analysis, related to Figure 2; Protein family = Protein family; Panther protein class = protein class retrieved from pantherdb.org; GO molecular function = Gene ontology molecular function; GO biological process = Gene ontology biological process; GO cellular component = Gene ontology cellular component.

Table S2 – Related to Figure 2. RNA binding proteins

Contains quantitative information about all RNA binding proteins (for column key see description of table S1).

Table S3 – Related to Figure 3. Protein families and complexes

Contains the information on coordinated proteome dynamics of protein families or proteins in complexes. Category = name of protein complex, protein family or gene ontology term; p.value = computed p-value for assessment of significance of co-regulation of the corresponding proteins. P-values were computed using the 'proteinProfile' package within R/bioconductor; ID = unique identified matching to table S1; Uniprot = Uniprot accession code; Gene.name = gene name; Protein.name = corresponding protein name; average log2 DIV5/DIV1 = the average log2 fold-change between DIV5 and DIV1; average log2 DIV14/DIV5 = the average log2 fold-change between DIV14 and DIV5.

Table S4 – Related to Figure 4. Synaptic proteins

Contains quantitative information about synaptic proteins (for column key see description of table S1).

Table S5 – Related to Figure 4. Cell adhesion proteins

Contains quantitative information about cell adhesion proteins (for column key see description of table S1).

Table S6 – Related to Figure 7. Interactors of NCAM1

Contains data from affinity purification mass spectrometry analysis of NCAM1 IPs in adult and young rat brain extracts. Uniprot = Uniprot accession code; gene name = gene name; Description = description of the protein; Σ# PSMs = sum of all peptide-spectrum-matches (PSMs) across all IPs; GFP_control = number of PSM from

GFP-only control IP; NCAM120/140/180 = number of PSM from NCAM120/NCAM140/NCAM180 IPs; p-value NCAM120/140/180 = probability score from SAINT (Significance Analysis of INTeractions, version 2.3.2, http://dx.doi.org/10.1038%2Fnmeth.1541) analysis. $0 \leq p \leq 1$, the higher the score the higher the probability for a given interaction with NCAM1; SAINT probability >0.75 = proteins with a SAINT probability score >0.75 are flagged as 'TRUE'.

SUPPLEMENTAL FIGURES

Figure S1, related to Figure 1, Frese et al.

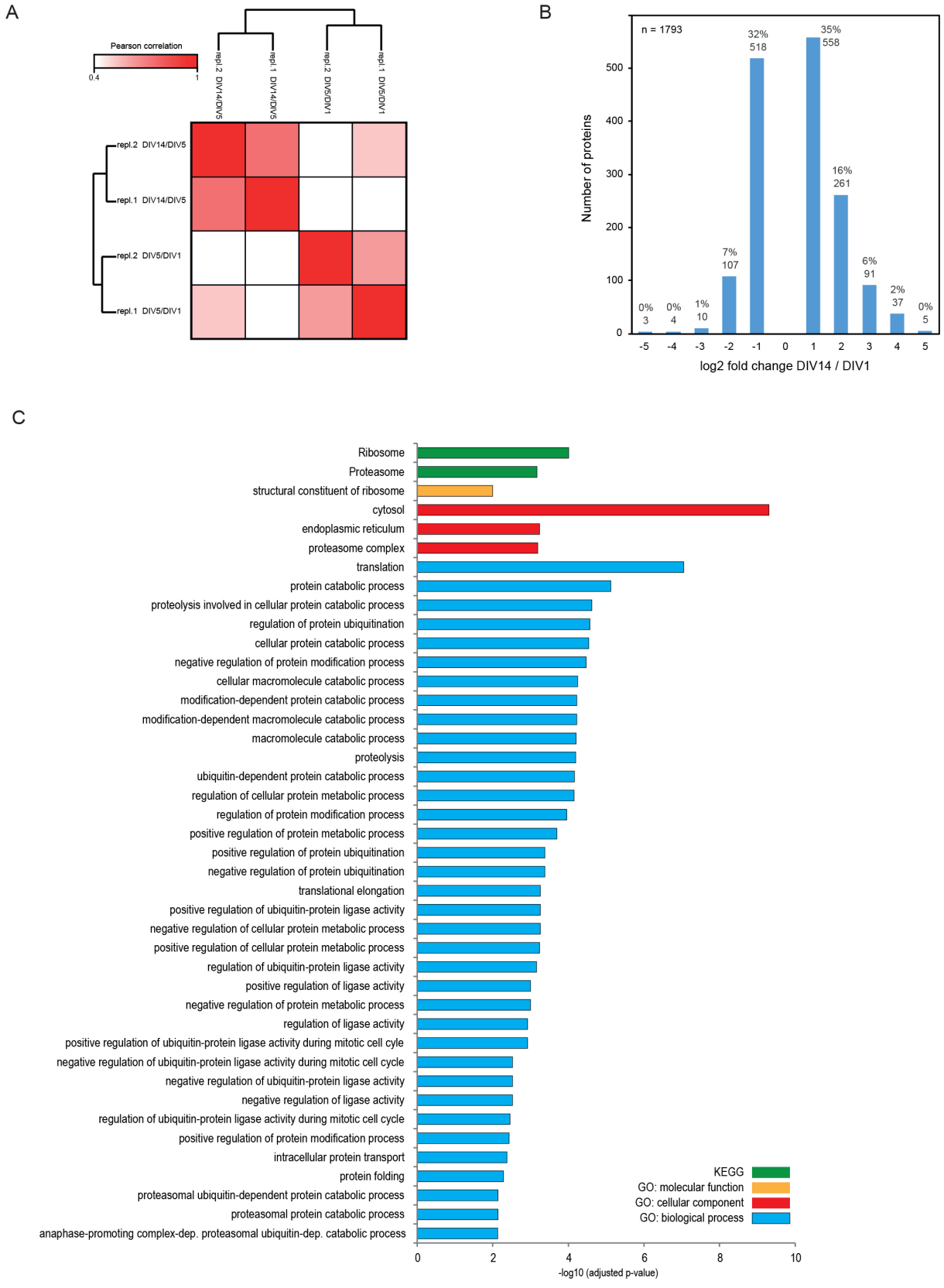

Figure S1 - Related to Figure 1. Reproducibility and statistical analysis of differentially expressed proteins

(A) Heat map showing Pearson correlation scores for the two independent biological replica.

(B) Distribution of fold changes calculated on all the quantified proteins.

(C) Gene ontology (GO) and KEGG pathway enrichment analysis. All quantified proteins were subjected to enrichment analysis with respect to biological process, molecular function, cellular component and protein class (KEGG).

Figure S2, related to Figure 2, Frese et al.

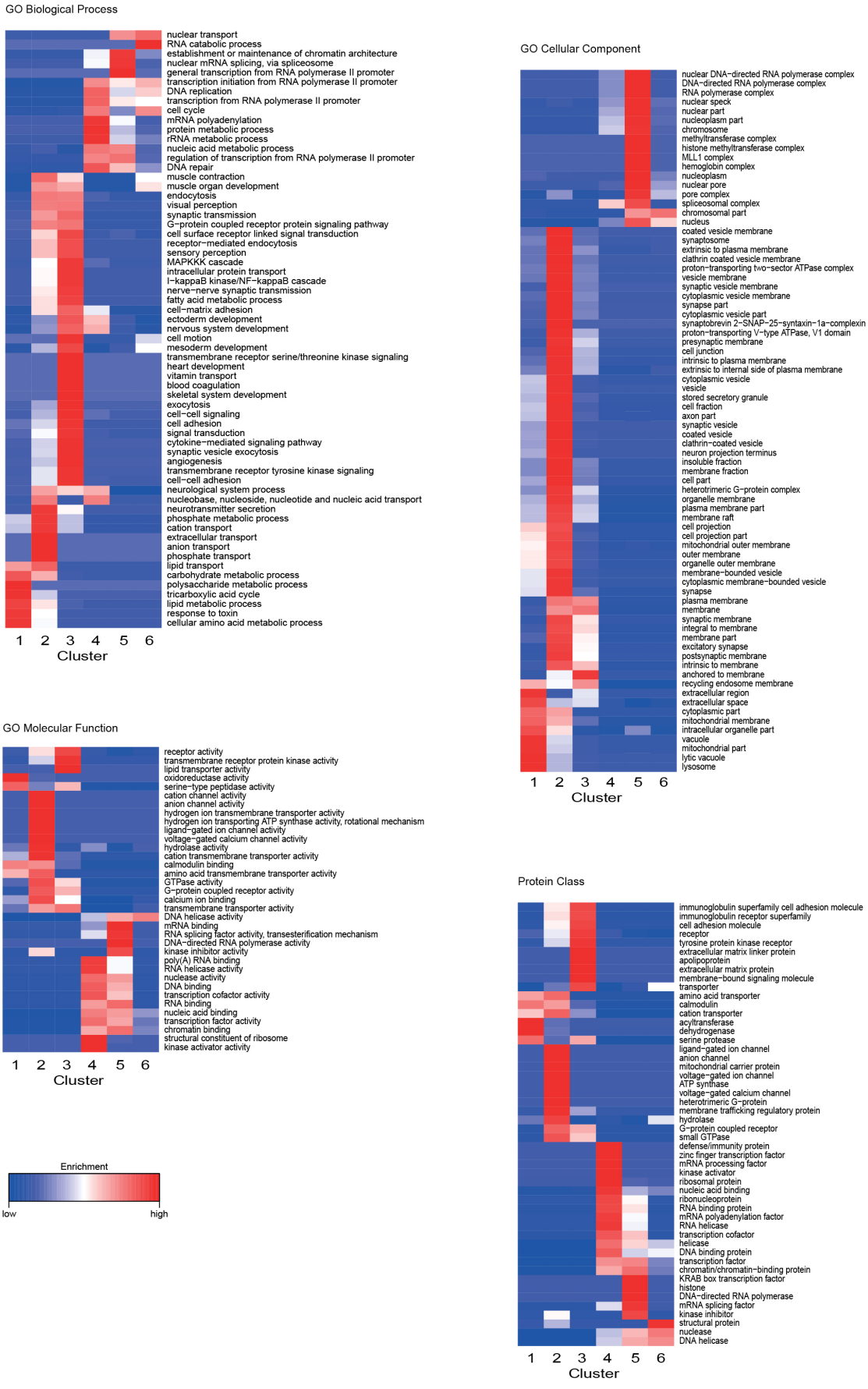

Figure S2 - Related to Figure 2. Gene ontology classification of regulated proteins

For all proteins of each cluster (see Figure 2) enrichment analysis with respect to biological process, molecular function, cellular component and protein class (KEGG) was performed. Overrepresentation was tested against all not regulated proteins. The heat maps show the overrepresentation /underrepresentation of each group in each specific cluster.

Figure S3, related to Figure 3, Frese et al.

A

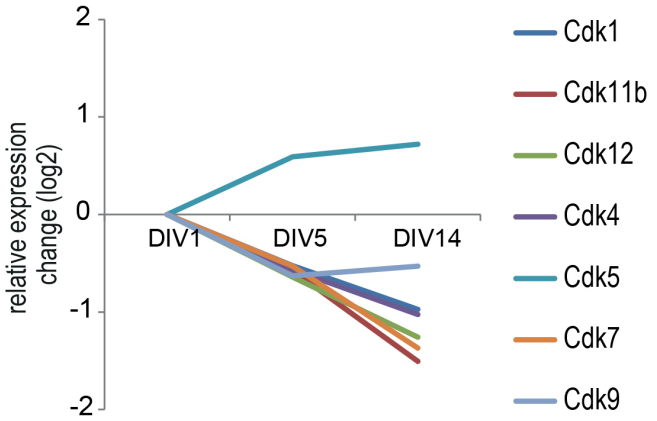

B

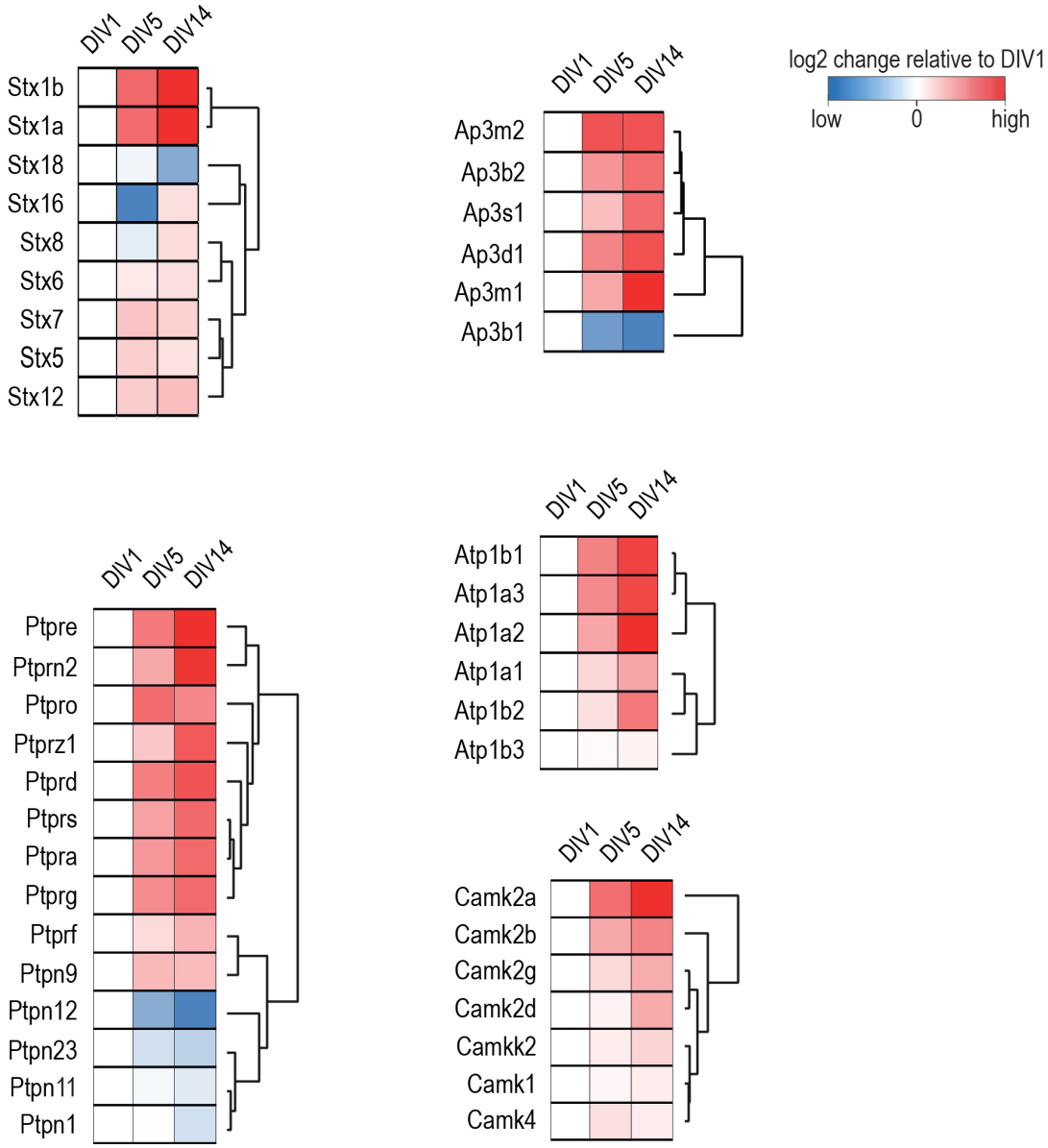

Figure S3 - Related to Figure 3. Expression profiles of protein families/complexes

(A) Expression profiles of proteins from the cyclin-dependent kinase family.

(B) Heat maps of expression profiles of proteins showed in Figure 3B. Ap3b1 (6 unique peptides used for the quantification) does not follow the expression profile of the other AP3 complex proteins. Similar trend has been measured for Atp1b3 (7 unique peptides used for the quantification) that does not change over time while other subunits of the complex are upregulated.

Figure S4, related to Figure 4, Frese et al.

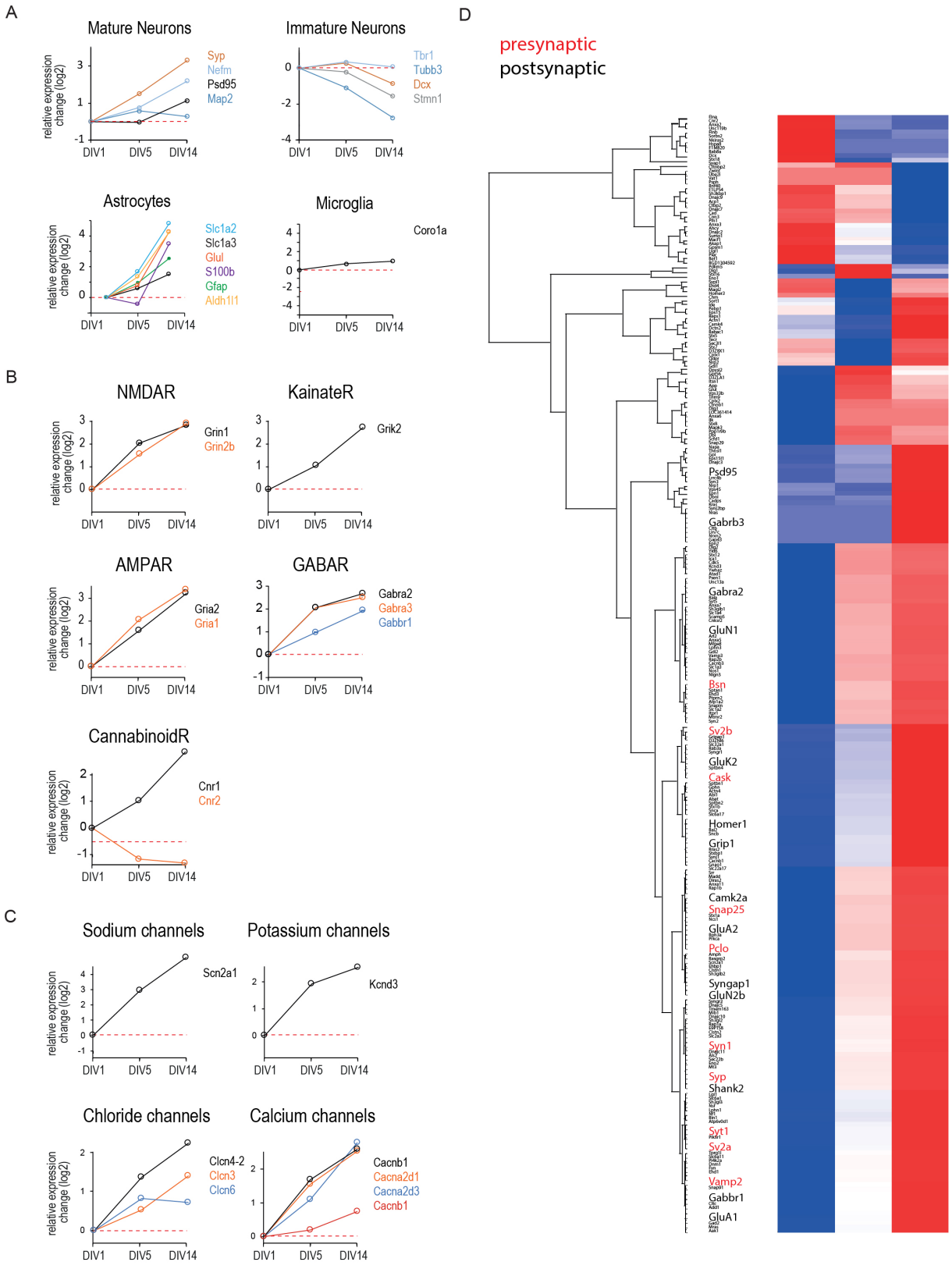

Figure S4 - Related to Figure 4. Expression profiles of cell-type protein markers and proteins with similar function/localization

(A) Expression profiles of selected protein markers for mature neurons, immature neurons, astrocytes and microglia. Astrocytes specific proteins are highly up-regulated after DIV5.

(B) Expression profiles of selected neurotransmitter receptors.

(C) Expression profiles of selected voltage-gated ion channels.

(D) Hierarchical clustering of all synaptic proteins (based on Euclidian distance). Proteins known to be located either pre- or postsynaptic are highlighted in bold. Evidently, the expression profiles of these two subclasses are not distinguishable by hierarchical clustering.

Figure S5, related to Figure 5, Frese et al.

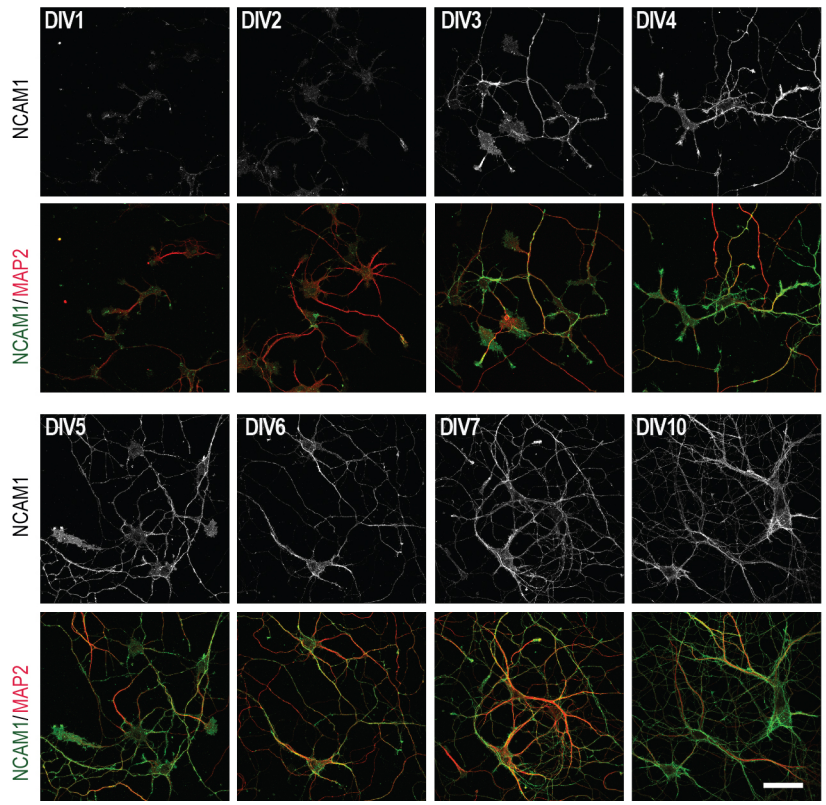

Figure S5 - Related to Figure 5. NCAM1 localization in mouse hippocampal primary neurons

Representative images of mouse hippocampal neurons from DIV1 to DIV10, stained for NCAM1 (green), MAP2 (red). Scale bar, 50 µm.

Figure S6, related to Figure 6, Frese et al.

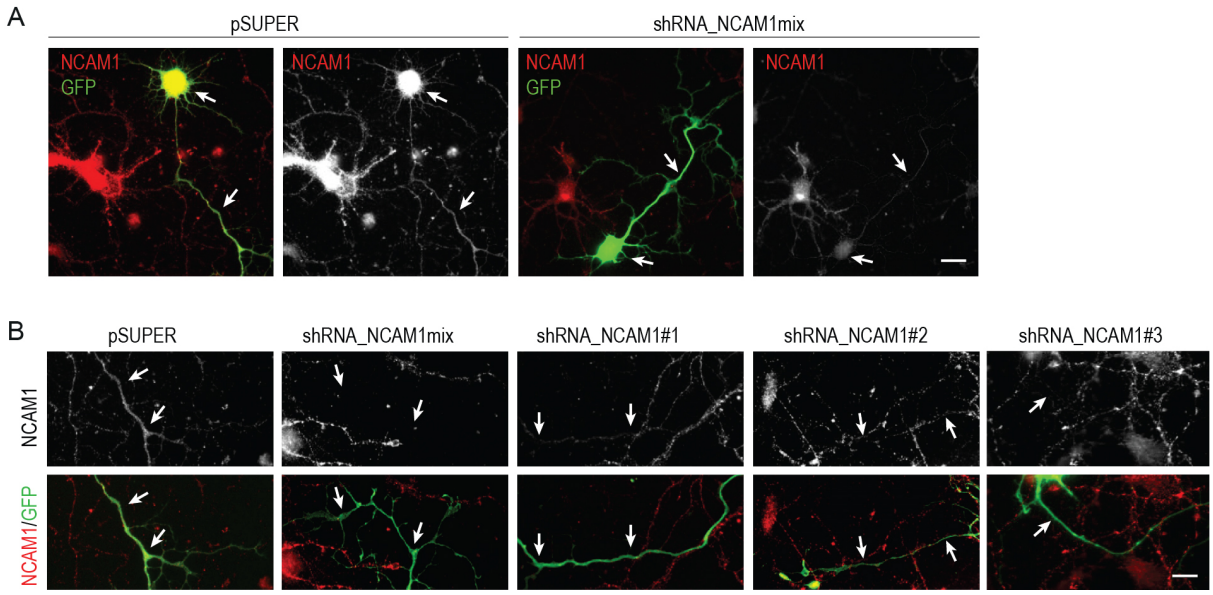

Figure S6 - Related to Figure 6. NCAM1 downregulation in rat hippocampal primary neurons

(A) Representative images of neurons transfected with pSUPER or shRNA NCAM1mix, filled with GFP (1DIV for 3 days) and stained with NCAM1 monoclonal antibody. Scale bar, 20 µm.

(B) Higher magnifications of representative images of neurons co-transfected with pSUPER, shRNA NCAM1mix, shRNA NCAM1#1, shRNA NCAM1#2, shRNA NCAM1#3 and GFP. Arrows point to representative neurites. Scale bar, 10 µm.

Figure S7, related to Figure 7, Frese et al.

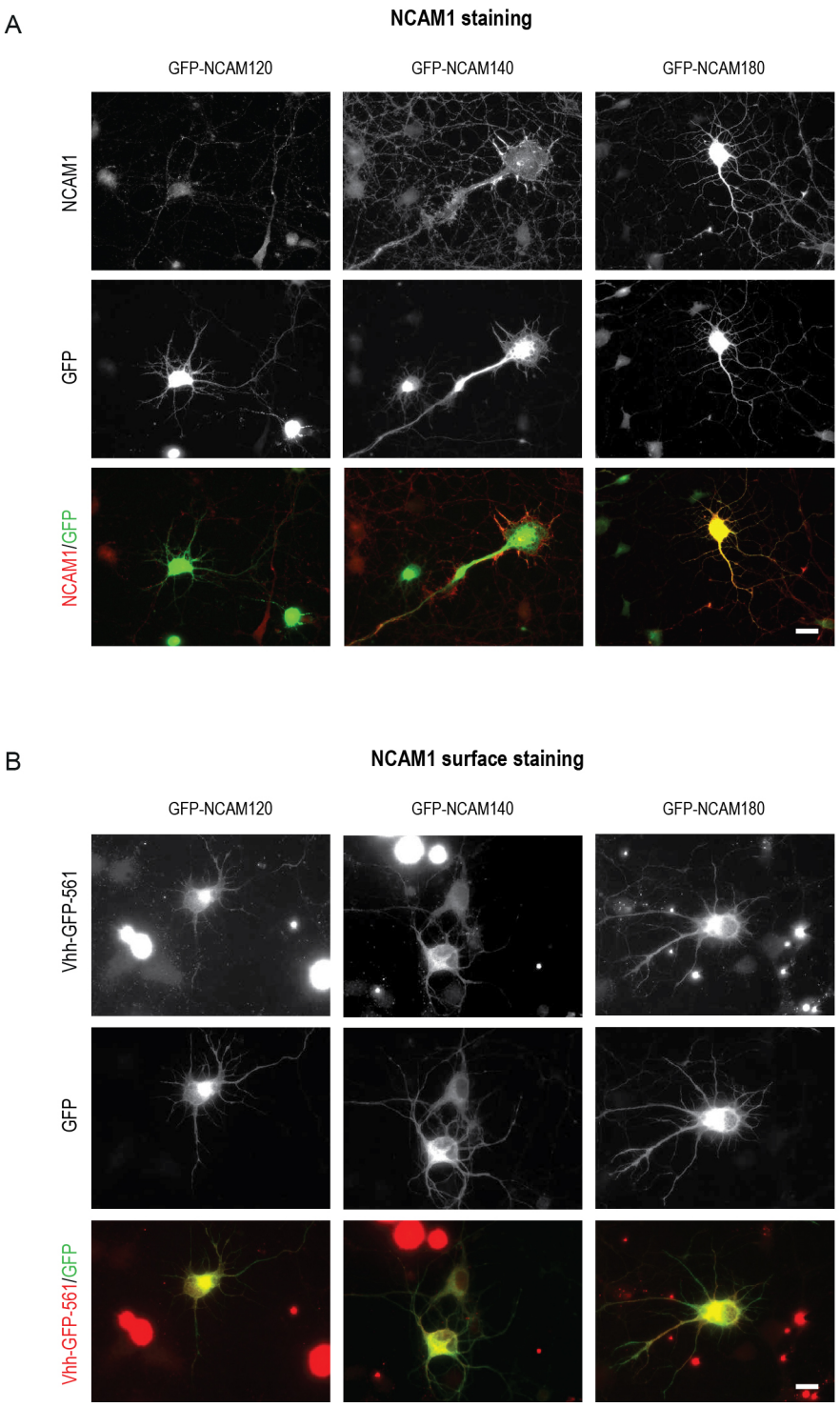

Figure S7 - Related to Figure 7. Characterization of N-terminal GFP tagged NCAM1 isoforms

(A) Representative images of neurons transfected with GFP-NCAM120, GFP-NCAM140 or GFP-NCAM180 and stained with NCAM1 mouse antibody. The NCAM1 antibody recognizes the C-terminal tail of NCAM1 and

as expected the signal is completely overlapping with the GFP only when the longer NCAM1 isoform (NCAM180) is expressed. Scale bar, 20 μm.
(B) Representative images of neurons transfected with GFP-NCAM120, GFP-NCAM140 or GFP-NCAM180 and live stained with Vhh-GFP-568 nanobodies. Cells were not permeabilized before the staining and the GFP-targeted-nanobodies were added directly in the medium at 37°C, so only NCAM1 molecules efficiently expressed on the neuronal surface can be detected. Scale bar, 10 μm.

SUPPLEMENTAL EXPERIMENTAL PROCEDURES

Animals

All experiments with animals were performed in compliance with the guidelines for the welfare of experimental animals issued by the Government of The Netherlands, and were approved by the Animal Ethical Review Committee (DEC) of the Utrecht University.

Antibodies and reagents

The following primary and secondary antibodies were used in this study: NCAM1 mouse (Millipore), NCAM1 rabbit (Proteintech), Syt1, Camk2a mouse (Sigma), PSD95, Cntn1, NCAM2, L1CAM, Kif5B, Actg mouse (Millipore) and Tubα1a rabbit (Abcam), MAP2 rabbit (Cell Signaling), Vhh-GFP-Alexa 561 nanobodies (Yau et al., 2014). Alexa 488-, Alexa 568- and Alexa 594-conjugated secondary antibodies (Invitrogen). Other reagents used in this study include: Jasplakinolide (2792, Tocris Bioscience), n-Dodecyl β-D-maltoside (A0819, Applichem).

Expression vectors and shRNA constructs

The following mammalian expression plasmids have been described: pGW1-GFP (Hoogenraad et al, 2005), pCDNA3.1-RFP-NCAM120, pCDNA3.1-RFP-NCAM140, pCDNA3.1-RFP-NCAM180, pCDNA3.1-eGFP-NCAM120, pCDNA3.1-eGFP-NCAM140, pCDNA3.1-eGFP-NCAM180 (Hata et al., 2007). The following shRNA sequences are used in this study. NCAM1#1 (5'-GGATCTCATCTGGACTTTG), NCAM1#2 (5'-GATCTTCCAGAAGCTCATG) and NCAM1#3 (CGTTGGAGAGTCCAAATTC) targeting rat NCAM1 mRNA (NM_031521.1) were designed using the siRNA selection program at the Whitehead Institute for Biomedical Research (jura.wi.mit.edu/bioc/siRNAext) (Yuan et al., 2004). The complementary oligonucleotides were annealed and inserted into a pSuper vector (Hoogenraad et al., 2005). The control pSuper vector contained a scrambled sequence.

Primary hippocampal neuron cultures and transfection

Rat primary hippocampal cultures were prepared from embryonic day 18 rat brains. Cells were plated on coverslips coated with poly-L-lysine (30μg /ml) and laminin (2μg/ml) at a density of 100,000/well as previously (Kapitein et al., 2010). Hippocampal cultures were grown in Neurobasal medium (NB) supplemented with B27, 0.5 μM glutamine, 12.5 μM glutamate and penicillin/streptomycin. Mouse primary hippocampal cultures were

prepared from embryonic day 18 mouse brains then plated and cultured in the same conditions as rat primary neurons.

Hippocampal neurons were transfected at DIV1 using Lipofectamine 2000 (Invitrogen). Briefly, DNA (1.8 µg/well, for a 12 wells plate) was mixed with 3.3 µl of Lipofectamine 2000 in 200µl NB, incubated for 30 min, and then added to the neurons in NB at 37°C in 5% CO2 for 45 min. Next, neurons were washed with NB and transferred in their original medium at 37°C in 5% CO2 for 3-7 days. For forced actin-stabilization experiments, young neurons co-transfected at day1 were treated 24 hours later (DIV2) with 10 nM Jasplakinolide and cells were then incubated for 6 days at 37°C in the presence of the drug (Swiech et al., 2011).

Primary cortical neuron nucleofection

Primary cortical neurons were isolated from E18 rat brain. Cells (1x106) were transfected using the Amaxa Rat Neuron Nucleofector kit (Lonza) with 3µg of plasmid DNA (pSUPER, ShRNA-NCAM1mix, ShRNA-NCAM1#1, ShRNA-NCAM1#2, ShRNA-NCAM1#3) and plated on coverslips coated with poly-L-lysine (37.5µg/ml) and laminin (5µg/ml) in 12-wells plates (2-6 x104 cells/well) containing DMEM supplemented with 10% FBS (Kaech and Banker, 2006). Cells were allowed to recover and adhere to the surface at 37°C in 5% CO2, after 4 hours the medium was replaced with Neurobasal medium supplemented with 2% B27, 0.5mM glutamine, 15.6µM glutamate, and 1% penicillin/streptomycin. After 4 days cells were lysed in hot denaturing sample buffer.

Sample preparation for Mass spectrometry

At three time points (DIV1, DIV5, DIV14) neurons were washed 4x with 500 µL pre-warmed PBS. For lysis 500 µL lysis buffer (8 M Urea, 1 tablet Complete Mini EDTA-free protease inhibitor Cocktail (Roche) in 10 mL 50 mM triethylammonium bicarbonate (Sigma)) was added to each well. Following sonication, samples were cleared by centrifugation at 20,000 × g for 20 min. Proteins were reduced (5 mM DTT, 55˚C, 30 min), alkylated (10 mM Iodoacetamide, 30 min in the dark) and sequentially digested by LysC (Protein-enzyme ratio 1:50, 37˚C, 4 h) and trypsin (Protein-enzyme ratio 1:50, 37˚C, 16 h) according to the standard filter-aided sample preparation protocol (Wiśniewski et al., 2009). Resulting peptides from each time point were desalted using C18 solid phase extraction cartridges (Waters) and subjected to stable isotope triplex dimethyl labeling on column (Boersema et al., 2009). Labels were swapped between biological replicates. Differentially labeled peptides were mixed in a 1:1:1 ratio based on LC-MS base peak intensity of the separate channels, dried in a vacuum concentrator and reconstituted in 10% formic acid for subsequent fractionation.

Peptide Fractionation

Peptides were fractionated using strong cation exchange chromatography (SCX), as previously described (Frese et al., 2012). Briefly, peptides were loaded onto a Zorbax BioSCX-Series II column (0.8 mm × 50 mm, 3.5 µm) in 100% solvent A (0.05% formic acid in 20% acetonitrile). Solvent B consisted of 0.05% formic acid and 0.5 M NaCl in 20% acetonitrile. Fractionation was conducted using the following gradient: 0−0.01 min (0−2% B); 0.01−8.01 min (2−3% B); 8.01−14.01 min (3−8% B); 14.01−28 min (8−20% B); 28−38 min (20−40% B); 38−48 min (40−90% B); 48−54 min (90% B); 54−60 min (0% B). Collected fractions were dried in vacuo, reconstituted in 10% formic acid/5% DMSO and stored at -80°C prior MS analysis.

Affinity Purification-Mass Spectrometry (AP-MS) using GFP pull-down

Human Embryonic Kidney 293 cells (HEK293) cells were cultured in DMEM/Ham's F10 (50%/50%) containing 10% Fetal Calf Serum (FCS) and 1% penicillin/streptomycin at 37°C and 5% CO2. HEK293 cells were transfected with pGW1-GFP, eGFP-NCAM120, eGFP-NCAM140 and eGFP-NCAM180 constructs with polyethylenimine (PEI, Polysciences) according to the manufacturer instructions. Cells were lysed 48 hours later in a lysis buffer for transmembrane proteins (20mM TrisHCl, 100mM NaCl, 10mM EDTA (pH8.0), 10mM Na4P2O7, 10% Glycerol, 50mM NaF, 1% n-Dodecyl β-D-maltoside, and protease inhibitors (Roche)), centrifuged at 13000 rpm for 15 min and the supernatants were incubated with GFP-trap beads (Chromotek) for 1 hour at 4°C. Beads were then separated using a magnet (Dynal; Invitrogen) and washed five times in washing buffer (20mM Tris HCl, 150mM KCl, 0.1% TritonX-100). Brains were obtained from female adult rats or P5 rat pups and homogenized in 10x volume/weight in tissue lysis buffer (50mM TrisHCl, 150mM NaCl, 0.1% SDS, 0.2% NP-40, and protease inhibitors (Roche)). Brain lysates were centrifuged at 16,000 g for 15 min at 4°C and the supernatant was incubated with the Dynabeads containing GFP or GFP-NCAM120/140/180 for 2 hrs at 4°C and washed with lysis buffer for five times. For MS analysis, the beads were resuspended in 15 ul of 4x Laemmli Sample buffer (Biorad) and supernatants were loaded on a 12% Criterion XT Bis-Tris precast gel (Biorad). The gel was stained with 0.1% Coomassie Brilliant Blue G250 (Sigma-Aldrich, Steinheim, Germany) in 25% methanol and 10% acetic acid (Merck, Darmstadt, Germany). Each lane from the gel was cut in 3 slices, destained and digested using trypsin, as described in (Ekkebus et al., 2013). Briefly, each lane from the gel was cut into three pieces and placed in 0.5-ml tubes. They were washed with 250 µl of water, followed by 15-min dehydration in acetonitrile. Proteins were reduced (10 mM dithiothreitol, 1h at 56°C), dehydrated and alkylated (55 mM iodoacetamide, 1h in the dark). After two rounds of dehydration, trypsin was added to the samples (20 µl of 0.1 mg/ml trypsin in 50 mM Ammoniumbicarbonate) and incubated overnight at 37°C. Peptides were extracted with ACN, dried down and reconstituted in 10% formic acid prior MS analysis.

Mass spectrometry analysis

All samples were analyzed on an ETD enabled LTQ-Orbitrap Elite or Q-Exactive mass spectrometer (Thermo Fisher Scientific, Bremen, Germany) that was coupled to Proxeon EASY-nLC 1000 (Thermo Fisher Scientific, Odense, Denmark). Peptides were loaded onto a trap column (Reprosil C18, 3 µm, 2 cm × 100 µm; Dr. Maisch) with solvent A (0.1% formic acid in water) at a maximum pressure of 800 bar and chromatographically separated over the analytical column (Zorbax SB-C18, 1.8 µm, 50 cm × 75 µm; Agilent) using a 60 min, 90 min or 150 min linear gradient from 7-30% solvent B (0.1% formic acid in acetonitrile) at a flow rate of 150 nL/min. The mass spectrometer was operated in the data-dependent acquisition mode. After a survey scan from 350-1500 m/z the 10 or 20 most abundant peptides were subjected to either HCD or decision tree-guided CID/ETD fragmentation (ddDT) (Frese et al., 2011), respectively. Product ions were detected in the Orbitrap (HCD methods; Resolution 7,500) and linear ion trap (ddDT methods), respectively. Normalized collision energy was set to 35% and 32% for CID and HCD, respectively. Charge state dependent ETD reaction time and supplemental activation were enabled. Charge state screening was enabled and ions with charge states <2+ were excluded from analysis. Samples from in-gel digestion were analyzed using a 90 min gradient.

Mass spectrometry data analysis

All mass spectrometric raw data were processed with Proteome Discoverer (version 1.3, Thermo Scientific, Bremen, Germany), as described in (Frese et al., 2012). Peak lists were generated using a standard workflow. The non-fragment filter was used to simplify ETD spectra. HCD spectra were deisotoped and charge deconvoluted. The TopN filter node was used to filter CID and ETD spectra and to retain the 10 most abundant peaks per 100 Da window. Peptide identification was performed by searching individual peak lists of HCD, ETD-IT and CID-IT against the Uniprot rat database (version 2013_01) concatenated with a list of common contaminants using Mascot (version 2.3, Matrix Science, UK). Trypsin was set as cleavage specificity, allowing a maximum of 2 missed cleavages. Precursor ion mass tolerance was set to 15 ppm. Product ion mass tolerance was set to 0.02 Da (Orbitrap detection) and 0.5 Da (ion trap detection), respectively. Carbamidomethylation (C) was used as fixed modification. Oxidation (M) and dimethylation (light, intermediate or heavy) of lysine residues and the peptide N-termini, respectively, were set as variable modification. The percolator algorithm was used to filter the data to <1% false-discovery-rate on peptide level. Additionally, only peptides that pass the following filters were retained: mascot ion score ≥20, minimum peptide length 6, precursor mass tolerance 10 ppm, and search engine rank 1. Only unique peptides were used for quantification and the obtained ratios were normalized to the median. AP-MS data was analyzed using Proteome Discoverer and the aforementioned settings. Common contaminant proteins including immunoglobulins were removed from the list.

Bioinformatic analysis

Gene ontology (GO) classification was obtained via PANTHER (Mi et al., 2005) and Perseus (version 1.3.0.4, within MaxQuant) (Cox et al., 2009). Enrichment analysis in terms of relative proteins abundance was performed using a Fisher's exact test in Perseus (GO cellular component, min. enrichment factor 3.5, Benjamini-Hochberg corrected p-value <0.02). KEGG pathway analysis and tissue enrichment testing were performed using DAVID (Cox et al., 2009) (Huang da et al., 2009). Hierarchical clustering was performed within Perseus using Euclidian distance. Network analysis was performed using the GeneMania plugin (Montojo et al., 2010) within Cytoscape (Shannon et al., 2003). Significance analysis of microarrays (SAM) (Roxas and Li, 2008) was used to assess significance of obtained protein ratios, as described in (Munoz et al., 2011). Briefly, log2-transformed ratios of proteins that were quantified in all time points and in both replicates were subjected to a one-class test using 1000 permutations and an S0 value based on the method by (Tusher et al., 2001). Proteins with a SAM q-value ≤0.15 (corresponding to a median log2 fold-change of >1.5 between DIV14 and DIV1) were considered significantly regulated and subjected to unsupervised fuzzy clustering using GProX 1.1.9 (Rigbolt et al., 2011). Briefly, the relative abundance of all proteins from each time point was log10 transformed, Z-scored and clustered using a fuzzification value of 2, 100 iterations and a minimum membership value of 0.35. Gene ontology enrichment for each cluster was performed using a Fisher's exact test within GProX (min. occurrences 5 for GOMF, GOBP and protein class, and 1 for GOCC; Benjamini-Hochberg corrected p-value <0.05). Significance of expression profile similarities within groups of interest was determined using the R package "proteinProfiles" (Julian Gehring [2011], https://bioconductor.org/packages/devel/bioc/html/proteinProfiles.html) within R/Bioconductor (Gentleman et al., 2004), as reported elsewhere (Hansson et al., 2012). The heatmap in Figure 7 was generated by subjecting log10-transformed and z-scored relative abundances of all proteins from each time point (DIV 1, 5, 14) to

hierarchical clustering using Euclidean distance. Statistical assessment of the AP-MS data was performed based on spectral counts using the SAINT (Significance Analysis of INTeractions, version 2.3.2) algorithm (Choi et al., 2011). The SAINT parameters were set as follows: nburn=4000, niter=20000, lowmode=0, minfold=1, and norm=1. Bait proteins with a SAINT probability score >0.75 were considered putative protein interaction partners.

Cell extracts and Western blotting

HEK293 cell extracts were prepared by resuspending cells in equal amounts of lysis buffer containing 25mM Tris-HCl pH 8.0, 50mM NaCl, 0.5% Triton X-100 supplemented with 1x protease inhibitors cocktail (Roche). The soluble fraction was separated by centrifugation at 13000 rpm for 15 minutes and supplemented with sample buffer 4x (8% SDS, 25% glycerol, 0.05M Tris pH 6.8, 400mM DTT and 40mg/l bromophenol blue). Rat primary hippocampal neurons (E18) were plated on 24 mm coverslips in 6 well plates and harvested at DIV 1, 5 and 14 days in vitro (DIV), or at DIV2, 4, 6, 8, 10, 12, 14, 16, 18 and 21. Cells were lysed in hot denaturing sample buffer. Lysates prepared from individual wells were pooled together (3 wells each stage, 3 independent preparations) and equal protein concentrations were adjusted before supplementing with 4x sample buffer. Samples were boiled at 99ºC for 10 minutes before being analyzed by SDS PAGE. Proteins were transferred on PVDF membranes (Millipore) using a semi-dry blotting system. Membranes were blocked and incubated with primary antibodies (overnight at 4°C) in PBS or PBST (0.1% Tween-20, 2% BSA). Peroxidase-coupled secondary antibodies were applied for 1 hour at RT. Following primary NCAM1 antibodies have been used for detection: NCAM1 mouse antibody (Millipore 1:1000), NCAM1 rabbit antibody (Proteintech 1:1000). For quantifying NCAM1 expression levels, the relative intensities of NCAM1 for each sample (n=3) were obtained by normalization to the tubulin loading control. The relative percentage of NCAM1 expression levels was obtained by normalization of the relative intensities with the relative intensity of NCAM1 at DIV2. For quantifying Syt1, Camk2a, PSD95, Cntn1, NCAM1, NCAM2, L1CAM expression levels, the relative intensities of each band (n=3) were measured together with 3 different loading controls such as Kif5B, Actg and Tubα1a . Quantifications were performed with Image J.

Immunohistochemistry

For general immunohistochemistry, neurons were fixed for 10 min with 4% paraformaldehyde (PFA)/4% sucrose in phosphate buffered saline (PBS) at room temperature. After fixation cells were washed 3 times for 10 min in PBS at room temperature, incubated for 10 min with permeabilization buffer (0.25% TritonX-100 in PBS) and then blocked for 1 hour with blocking buffer (2% BSA, 2% Glycin, 0.2% Gelatin, 50mM NH4Cl, in PBS). Neurons were then incubated with primary antibodies in blocking buffer overnight at 4°C, washed three times in PBS for 10 min at room temperature and then incubated with the Alexa-conjugated secondary antibodies in blocking buffer for 1 hour at room temperature. Neurons were then washed 3 times for 5 min in PBS at room temperature and subsequently mounted on slides in Vectashield mounting medium (Vector Laboratories). For labeling of F-actin neurons were incubated with Phalloidin-647 (1:100 in PBS; Molecular Probes) for 30 min at room temperature, washed 3 times in PBS and mounted on slides in Mowiol. Images were acquired using a Nikon upright or Olympus BX53 upright fluorescent microscopes with a 10x, 20x or 40x objective. Confocal images were acquired using a Leica SP5 microscope (Wetzlar, Germany) equipped with a

Krypton-Argon-Ion laser (488/568/647 nm) and an acousto-optic-tunable filter (AOTF) for selection and intensity adaptation of laser lines. Images and were taken with 63x oil objective as z-stacks (300 nm z-step) and maximum intensity projections were calculated from each fluorescence channel of the image-stack.

Analyzing NCAM1 knockdown efficiency by immunostaining

Efficiency of NCAM1 shRNA knock down was verified by immunostaining of endogenous NCAM1 protein in hippocampal neurons co-transfected at DIV1 with 0.45 µg/well GFP and 1,35 µg/well of different NCAM1-shRNAs or a mixture of all of them, and fixed 3 days later. NCAM1 staining was measured in neurites of GFP positive neurons and was compared to NCAM1 staining in neurites of GFP negative surrounding cells. Quantifications were performed with Image J software (http://rsb.info.nih.gov/ij).

Quantification of fluorescent intensity. For the quantification of antibody staining, images were acquired with a 40x oil objective with the same settings and the exposure time and ImageJ was used to manually draw specific regions of interest (ROI) located in primary neurites. From the ROIs the mean intensity was measured. To prevent selection bias during quantification, in NCAM1-KD neurons the neurites segments were selected in one channel (GFP) and blindly quantified in the other channel (NCAM1 intensity). Intensities were measured in at least three neurites per neuron, in segments of approximately the same size, both in GFP positives and GFP negatives neurons within the image. To remove the background signal, the intensity near the selected neurites (same segment size) was measured and subtracted to the neurites measured intensities within the same image. Intensities were averaged over multiple cells, normalized and a statistical analysis was performed with student's t test assuming a two-tailed and unequal variation. For Figure 6C, n = 9+9 neurons for pSUPER, n = 13+13 neurons for shNCAM1 mix, n = 7+7 neurons for shNCAM1#1, #2 and #3. n is derived from two independent experiments.

Morphometric analyses of hippocampal neurons

To analyze axonal and dendritic morphology of NCAM1 knockdown neurons, GFP was used as an unbiased cell-fill in combination with different NCAM1-shRNAs or a mixture of all of them. Hippocampal neurons were co-transfected at DIV1 using the same concentrations of plasmid DNA previously reported, and fixed 7 days later. The morphometric analysis and quantification were performed with ImageJ. The axonal parameters, such as axonal total length and longest neurite length, were measured in images acquired with a dry 10x objective whereas quantification of the dendrites total length, primary dendrites length and branches length was done with images acquired with an 20x dry or 40x oil objective. For axon and dendrite length, all neurites of a single neuron were traced in ImageJ and the number of pixels was then converted to distance in µm. Morphological characteristics and MAP2 staining were used as parameters to distinguish axon and dendrites. Data were averaged over multiple cells and experiments, and a statistical analysis was performed with student's t-test assuming a two-tailed and unequal variation. For Figure 6E (axon morphology); n = 18 neurons for pSUPER, n = 25 neurons for shNCAM1mix, n = 17 neurons for shNCAM1#1, n = 16 neurons for shNCAM1#2, n = 18 neurons for shNCAM1#3. For Figure 6F (dendrites morphology): n = 9 neurons for pSUPER, n = 10 neurons for shNCAM1mix, n = 8 neurons for shNCAM1#1, n = 8 neurons for shNCAM1#2, n = 9 neurons for shNCAM1#3. For Figure 7F (axon morphology): n = 9+9 neurons for pSUPER, n = 9+9 neurons for shNCAM1#1, n = 11+11

neurons for shNCAM1#3. For Figure 7G (dendrites morphology): n = 12+12 neurons for pSUPER, n = 12+12 neurons for shNCAM1#1, n = 13+13 neurons for shNCAM1#3. n is derived from two independent experiments.

SUPPLEMENTAL REFERENCES

Boersema, P.J., Raijmakers, R., Lemeer, S., Mohammed, S., and Heck, A.J.R. (2009). Multiplex peptide stable isotope dimethyl labeling for quantitative proteomics. Nat. Protoc. *4*, 484–494.

Choi, H., Larsen, B., Lin, Z.Y., Breitkreutz, A., Mellacheruvu, D., Fermin, D., Qin, Z.S., Tyers, M., Gingras, A.C., and Nesvizhskii, A.I. (2011). SAINT: probabilistic scoring of affinity purification-mass spectrometry data. Nat. Methods *8*, 70–73.

Cox, J., Matic, I., Hilger, M., Nagaraj, N., Selbach, M., Olsen, J. V, and Mann, M. (2009). A practical guide to the MaxQuant computational platform for SILAC-based quantitative proteomics. Nat. Protoc. *4*, 698–705.

Ekkebus, R., Van Kasteren, S.I., Kulathu, Y., Scholten, A., Berlin, I., Geurink, P.P., De Jong, A., Goerdayal, S., Neefjes, J., Heck, A.J.R., et al. (2013). On terminal alkynes that can react with active-site cysteine nucleophiles in proteases. J. Am. Chem. Soc. *135*, 2867–2870.

Frese, C.K., Altelaar, A.F.M., Hennrich, M.L., Nolting, D., Zeller, M., Griep-Raming, J., Heck, A.J.R., and Mohammed, S. (2011). Improved Peptide Identification by Targeted Fragmentation Using CID, HCD and ETD on an LTQ-Orbitrap Velos. J. Proteome Res. *10*, 2377–2388.

Frese, C.K., Altelaar, A.F.M., Van Den Toorn, H., Nolting, D., Griep-Raming, J., Heck, A.J.R., and Mohammed, S. (2012). Toward full peptide sequence coverage by dual fragmentation combining electron-transfer and higher-energy collision dissociation tandem mass spectrometry. Anal. Chem. *84*, 9668–9673.

Gentleman, R.C., Carey, V.J., Bates, D.M., Bolstad, B., Dettling, M., Dudoit, S., Ellis, B., Gautier, L., Ge, Y., Gentry, J., et al. (2004). Bioconductor: open software development for computational biology and bioinformatics. Genome Biol. *5*, R80.

Hansson, J., Rafiee, M.R., Reiland, S., Polo, J.M., Gehring, J., Okawa, S., Huber, W., Hochedlinger, K., and Krijgsveld, J. (2012). Highly Coordinated Proteome Dynamics during Reprogramming of Somatic Cells to Pluripotency. Cell Rep. *2*, 1579–1592.

Hata, K., Polo-Parada, L., and Landmesser, L.T. (2007). Selective targeting of different neural cell adhesion molecule isoforms during motoneuron myotube synapse formation in culture and the switch from an immature to mature form of synaptic vesicle cycling. J. Neurosci. *27*, 14481–14493.

Hoogenraad, C.C., Milstein, A.D., Ethell, I.M., Henkemeyer, M., and Sheng, M. (2005). GRIP1 controls dendrite morphogenesis by regulating EphB receptor trafficking. Nat. Neurosci. *8*, 906–915.

Huang da, W., Sherman, B.T., and Lempicki, R.A. (2009). Systematic and integrative analysis of large gene lists using DAVID bioinformatics resources. Nat. Protoc. *4*, 44–57.

Kapitein, L.C., Yau, K.W., and Hoogenraad, C.C. (2010). Microtubule Dynamics in Dendritic Spines. Methods Cell Biol *97*, 111-132.

Mi, H., Lazareva-Ulitsky, B., Loo, R., Kejariwal, A., Vandergriff, J., Rabkin, S., Guo, N., Muruganujan, A., Doremieux, O., Campbell, et al. (2005). The PANTHER database of protein families, subfamilies, functions and pathways. Nucleic Acids Res. *33*, D284-288.

Montojo, J., Zuberi, K., Rodriguez, H., Kazi, F., Wright, G., Donaldson, S.L., Morris, Q., and Bader, G.D. (2010). GeneMANIA cytoscape plugin: Fast gene function predictions on the desktop. Bioinformatics *26*, 2927–2928.

Munoz, J., Low, T.Y., Kok, Y.J., Chin, A., Frese, C.K., Ding, V., Choo, A., and Heck, A.J.R. (2011). The quantitative proteomes of human-induced pluripotent stem cells and embryonic stem cells. Mol. Syst. Biol. *7*, 1–13.

Rigbolt, K.T.G., Vanselow, J.T., and Blagoev, B. (2011). GProX, a user-friendly platform for bioinformatics analysis and visualization of quantitative proteomics data. Mol. Cell. Proteomics *10*, O110.007450.

Roxas, B.A., and Li, Q. (2008). Significance analysis of microarray for relative quantitation of LC/MS data in proteomics. BMC Bioinformatics *9*, 187.

Shannon, P., Markiel, A., Ozier, O., Baliga, N.S., Wang, J.T., Ramage, D., Amin, N., Schwikowski, B., and Ideker, T. (2003). Cytoscape: A software Environment for integrated models of biomolecular interaction networks. Genome Res. *13*, 2498–2504.

Swiech, L., Blazejczyk, M., Urbanska, M., Pietruszka, P., Dortland, B.R., Malik, A.R., Wulf, P.S., Hoogenraad, C.C., and Jaworski, J. (2011). CLIP-170 and IQGAP1 cooperatively regulate dendrite morphology. J. Neurosci. *31*, 4555–4568.

Tusher, V.G., Tibshirani, R., and Chu, G. (2001). Significance analysis of microarrays applied to the ionizing radiation response. Proc. Natl. Acad. Sci. USA *98*, 5116–5121.

Wiśniewski, J.R., Zougman, A., Nagaraj, N., and Mann, M. (2009). Universal sample preparation method for proteome analysis. Nat. Methods *6*, 359–362.

Yuan, B., Latek, R., Hossbach, M., Tuschl, T., and Lewitter, F. (2004). siRNA selection server: An automated siRNA oligonucleotide predicition server. Nucleic Acids Res. *32*, W130-134.